IEEE Access
Multidisciplinary | Rapid Review | Open Access Journal

Received 7 June 2022, accepted 19 June 2022, date of publication 23 June 2022, date of current version 5 July 2022.

Digital Object Identifier 10.1109/ACCESS.2022.3185656

Integration of Small Productive Processes Into an Energy Management System for Microgrids

DANNY ESPIN-SARZOSA[1,2], (Member, IEEE), RODRIGO PALMA-BEHNKE[1,2], (Senior Member, IEEE), AND FELIPE VALENCIA[3,4], (Member, IEEE)

[1]Department of Electrical Engineering, Faculty of Physical and Mathematical Sciences, University of Chile, Santiago 8370451, Chile
[2]Energy Center, Faculty of Physical and Mathematical Sciences, University of Chile, Santiago 8370450, Chile
[3]Facultad de Ciencias de la Ingeniería, Universidad Austral de Chile, Valdivia 5090000, Chile
[4]Facultad de Minas, Universidad Nacional de Colombia, Medellín 050001, Colombia

Corresponding author: Rodrigo Palma-Behnke (rodpalma@cec.uchile.cl)

This work was supported in part by the Chilean National Agency of Research and Development (ANID) through the Comisión Nacional de Investigación Científica y Tecnológica-Programa de Formación de Capital Humano Avanzado (CONICYT-PFCHA), Doctorado Nacional, under Grant 2017-21171695; in part by the Solar Energy Research Center (SERC) Chile Fondo de Financiamiento de Centros de Investigación en Áreas Prioritarias (FONDAP)/CONICYT under Grant 15110019; and in part by Fondo Nacional de Desarrollo Científico y Tecnológico (FONDECYT) under Grant 1211968. The work of Felipe Valencia was supported by the Program "Estrategia de Transformación del Sector Energético Colombiano en el Horizonte de 2030" funded by Colciencias through the Grant 778 Ecosistema Científico under Contract FP44842-210-2018.

ABSTRACT Small productive processes (SPPs) have recently emerged as attractive alternatives to contribute to the socio-economic development of communities, primarily in rural contexts. However, SPPs have a complicated electrical behavior involving the interaction between various types of loads, such as, conventional, and complex ones. Further, the SPPs generally include voltage-dependent loads, which may increase/decrease the load consumption. Thus, these characteristics make the integration of the SPPs into energy management systems (EMSs) for microgrids a challenging task. This work proposes a novel integration of the SPPs into an EMS considering the SPPs' voltage sensitivity and complexity. For this purpose, we enhanced a previously proposed extended multi-zone ZIP load model (EMZ-ZIP) to be integrated into a convex AC multi-nodal EMS approach. The latter was formulated based on invertible nonlinear convex transformations and a binomial approximation method. The associated framework was assessed using a modified 9-bus test system with the characteristics of a low-voltage isolated microgrid with the integration of an SPP. The results demonstrate that the microgrid operation exhibits better technical and economic performance when the EMZ-ZIP model is an integral part of the EMS. In addition to an operating cost reduction of approximately 5% when considering voltage dependency, relevant practical advantage in scenarios of work shift and solar radiation variability are also presented. These results were compared with those obtained using other approaches like the time-variant ZIP and the constant power model.

INDEX TERMS Convex optimization, energy management system, microgrid, multi-zone ZIP load model, small productive processes.

NOMENCLATURE

SUBSCRIPTS AND SETS

$b \in \mathcal{B}$	Battery energy storage system.
$g \in \mathcal{G}$	Thermal generator.
$k \in \mathcal{K}$	Scheduling time horizon, $\mathcal{K} = \{1, \ldots, K\}$.
$n \in \mathcal{N}$	Load center.
$\omega \in \Omega$	Set of small productive processes' active devices.
$r, s \in \mathfrak{B}$	Set of system buses.

PARAMETERS

A_{PV}	Total photovoltaic plant surface.
B	Line conductance.
C_g	Generation costs of *g-th* thermal generator.
C_b	Operating costs of *b-th* battery unit.
C_{US}	Cost of the unserved power in the system.
E_b^{init}	Initial stored energy by the *b-th* battery unit.
E_b^{min}, E_b^{max}	Minimum and maximum allowed values of energy stored by the *b-th* battery unit.
G	Line susceptance.

The associate editor coordinating the review of this manuscript and approving it for publication was Qiang Li.

P_g^{min}, P_g^{max}	Minimum and maximum limits of active power generated by the *g-th* thermal generator.
$P_{ch,b}^{max}$, $P_{dis,b}^{max}$	Maximum charging and discharging allowed values of active power of the *b-th* battery unit.
$P_{L,n}$	Load consumption in the *n-th* load center of the system.
$P_{0,\omega}$	Nominal active power of the *ω-th* active device of the small productive process.
R	Line resistance.
$S_{r,s}^{max}$	Maximum limit of apparent power of lines.
V_0	Nominal voltage.
V_r^{min}, V_r^{max}	Minimum and maximum limits of voltages at the *r-th* bus.
X	Line reactance.
Y_{bus}	Admittance matrix.
ZIP_ω	ZIP load model of the *ω-th* active device of the small productive process.
$\alpha_{1,\omega}$	Constant-impedance characteristic of the *ω-th* active device of the SPP.
$\alpha_{2,\omega}$	Constant-current characteristic of the *ω-th* active device of the small productive process.
$\alpha_{3,\omega}$	Constant-power characteristic of the *ω-th* active device of the small productive process.
$\Im(Y_{r,s})$	Imaginary part of the admittance matrix.
Δ_k	Duration of time sub-period *k*.
η_b^{ch}, η_b^{dis}	Battery energy storage's charging efficiency and discharging efficiency.
η_{PV}	Solar panel efficiency.
$\Re\left(Y_{r,s}\right)$	Real part of the admittance matrix.
v_g^{min}, v_g^{max}	Minimum and maximum volume of the fuel tank of the *g-th* thermal generator.
Ψ	Solar radiation.

VARIABLES

E_b	Energy stored in the *b-th* battery unit.
E_b^{final}	Final energy stored by the *b-th* battery unit.
$I_{r,s}$, $T_{r,s}$	Auxiliary variables for the convex transformation of network constraints.
P_g	Active power of the *g-th* thermal generator.
P_b	Injected/consumed active power by the *b-th* battery unit.
P_b^{ch}, P_b^{dis}	Charging and discharging power of the *b-th* battery unit.
P_{flex}	Nominal active power of the flexible component.
$P_{DG,m}$	Active power supplied by the *m-th* distributed generator.
P_{US}	Unserved power in the system.
P_{PV}	Active power provided by the PV plant.
P_r, Q_r	Difference between generated and demanded power at the *r-th* bus.
$P_{r,s}$, $Q_{r,s}$, $S_{r,s}$	Active, reactive, and apparent power from bus *r* to bus *s*.
$P_{r,s}^{loss}$, $Q_{r,s}^{loss}$	Active and reactive power losses of system lines.
P_{SPP}, Q_{SPP}	Active and reactive power consumed by the small productive process.
Q_g	Reactive power of the *g-th* thermal generator.
u_r	Auxiliary variable for voltage squared at the *r-th* bus.
v_g	Volume of the fuel tank of the *g-th* thermal generator.
V	Measured voltage.
$\tilde{V}$	Ratio between measured voltage and nominal voltage.
V_r	Voltage at bus *r*.
y_b^{ch}, y_b^{dis}	Charging and discharging binary variables of the *b-th* battery unit.
ZIP_{flex}	Flexible component of the extended multi-zone ZIP load model.
$\tilde{\alpha}_1$	Constant-impedance characteristic of the flexible component.
$\tilde{\alpha}_2$	Constant-current characteristic of the flexible component.
$\tilde{\alpha}_3$	Constant-power characteristic of the flexible component.
δ_ω	Contribution of the *ω-th* active device to the total load consumption of the small productive process.
$\zeta_{r,s}$	Current flowing through the system lines.
$\ell_{r,s}$	Current squared.
θ_r	Angle at the *r-th* bus.
ψ	Time zone.

ACRONYMS

AC	Alternating Current.
ANN	Artificial Neural Network.
BAM	Binomial Approximation Method.
BESS	Battery Energy Storage System.
CLP	Chilean Pesos.
CP	Constant-power load model.
DC	Direct Current.
DER	Distributer Energy Resources.
DG	Distributed Generator.
DGU	Diesel Generator Unit.
EMS	Energy Management System.
EMZ-ZIP	Extended Multi-Zone ZIP load model.
GO	Global Optimization.
LV	Low voltage.
MG	Microgrid.
MILP	Mix-integer Linear Programming.
MPPT	Maximum Power Point Tracker.
NG	Nanogrid.
PUE	Productive Use of Energy.
PV	Photovoltaic.
RES	Renewable Energy Sources.
SDG	Sustainable Development Goals.
SOCP	Second-order Cone Programming.
SPP	Small Productive Process.

TAM	Taylor series Approximation Method.
TV-ZIP	Time-variant ZIP load model.
VPP	Virtual Power Plant.
VSC	Voltage Source Converter.
ZIP	Constant-impedance, constant-current and constant-power characteristics of a load.

I. INTRODUCTION

Small productive processes (SPPs) have recently emerged as appealing alternatives to contribute to the socio-economic development of communities, especially in rural contexts [1], [2]. This is due to their efficient use of the productive use of energy (PUE). Additionally, SPPs have included renewable energy sources (RES) [3], [4] to mitigate the effects of climate change. Further, due to their scalability, competitive investment costs and flexible operation [5], microgrids (MGs) have been one of the most popular choices for taking advantage of local RES [6]. For these reasons, both SPPs and MGs play a key role in contributing to the United Nations' sustainable development goals (SDG) [7].

PUE can be defined as "agricultural, commercial, and industrial activities involving electricity services as a direct input to the production of goods or provision of services" [8]. In developing countries, typical examples of PUE can be found in agro-processing, different manufacturing industries, for instance, welding, tailoring, among others [1]. In this context, SPPs can be defined as small manufacturing industries that aim to increase the income and productivity of people in, primarily rural communities, along with achieving the SDG.

Due to the previously mentioned benefits, several initiatives have been around the world to further explore the use SPPs. In [9], the authors present some examples of the SPPs that provide economic benefits to people in rural communities. For example, ice making, milling, carpentry, egg incubation, and water treatment. In [1], a description of other examples of SPPs such as grain milling, carpentry, tailoring, welding, among others, is provided. Moreover, in [10], the authors summarize examples of several SPPs worldwide, primarily in developing countries, that have helped the local communities in a socio-economic manner. In Chile, several solar-based SPPs have been installed in the northern part of the country. For instance, camelid fiber processing [11], farming of river shrimp, processing of agricultural products, among others [12]. Those SPPs have a complex electrical behavior involving the interaction between various types of loads [13]. Further, SPPs generally include voltage-dependent loads, which may change the expected load consumption [14].

MGs are generally low-voltage (LV) electrical systems that comprise distributed energy resources (DER) (e.g., diesel generators, micro-turbines, fuel cells, photovoltaic (PV) plants, etc.), storage units (e.g., batteries, flywheels, etc.), and loads [15] (e.g., conventional, flexible, and more recently, the SPPs [4]), which operate locally as a single controllable entity [16]. A MG can operate in either on-grid or off-grid mode. In on-grid mode, the main grid maintains its frequency and voltage within normal operating ranges. While in off-grid mode (islanding), the local generation units perform the frequency and voltage control of the MG. Islanding MGs are typically weak networks that can suffer from voltage fluctuations [17]. During islanding mode, the frequency and voltage in the MG is prone to more fluctuations due to power balance mismatches [18]. Besides, regardless of the operation mode, MGs present a low X/R ratio. Thus, load variations and the variability of RES injections can significantly impact the voltage profile [19].

Based on its previous definition, an SPP comprises of a complex cluster of loads associated to a specific location and industrial process. Thus, it does not require local distributed generation (DG). Nevertheless, some SPPs may include DG and storage units. In the latter case, as shown in Fig. 2, an SPP has certain relationships with other systems such as MG, nanogrid (NG), and virtual power plant (VPP). When an SPP includes local generation, storage, and the capability of autonomous operation, it can be considered as a MG. In the case of an SPP for a very small manufacturing process with MG capabilities (local controller) it can be considered a NG [20]. Finally, if one or several SPPs contain local generation and storage they can also participate and be coordinated as part of a VPP. In this case, they will be managed by an energy management system (EMS) which is the heart of the VPP [21].

The bulk power system, and primarily the MGs, will include more and more diverse electrical loads, from small local applications to complex structures (i.e., SPPs) that will integrate different types of activities (domestic, industrial processes, etc.) This future scenario is exemplified in Fig. 1. In addition, the concept of networked MGs (i.e., two or more MGs connected to the main grid) has emerged as an attractive alternative to solve the seamless transition and grid-connected operation of numerous and various distributed energy sources [22]. In this context, there are MGs that can be used for residential, commercial, and industrial purposes [23]. Therefore, having a better understanding and representation of their internal loads will contribute the EMS make better decisions [22] to assist the decision maker and the system tools.

An EMS is responsible for determining the optimal (near optimal) operating set points of dispatchable units in a MG [5] by solving a unit commitment and/or an economic dispatch problem [24]. For this purpose, an EMS considers different information such as load forecasting, power generation available from DER, energy available from storage, weather forecasts, energy prices, etc. [25]. However, when having complex loads (i.e., SPPs), their representation and integration into an EMS is a challenging task.

For example, in [26], an EMS that manages the operation of a MG and considers a small copper mining process is proposed. In [27], the scheduling of units in a rural MG that includes residential loads, and an agricultural production process is presented. The authors in [28] present the design of the operation of a MG, based mainly on solar

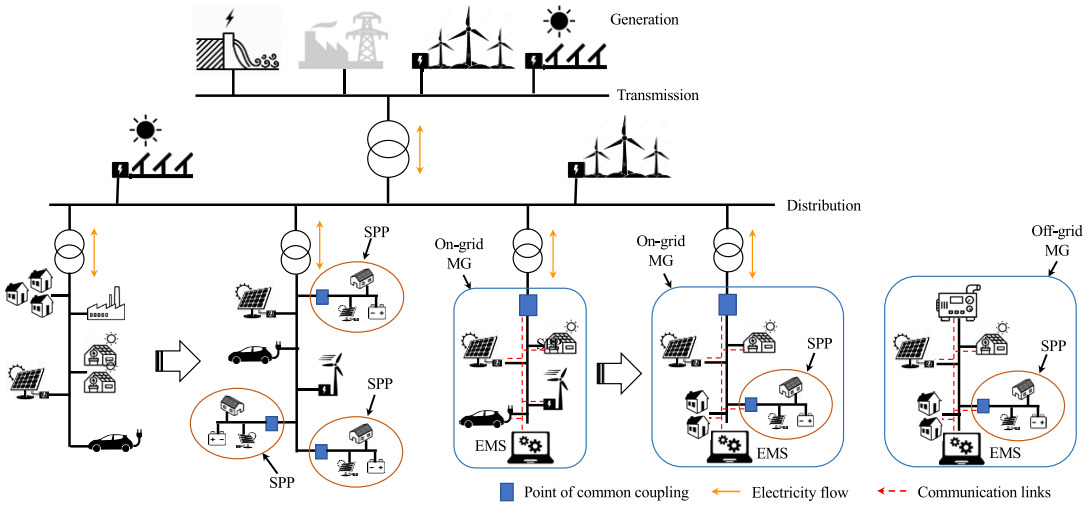

FIGURE 1. Future electrical systems including SPPs.

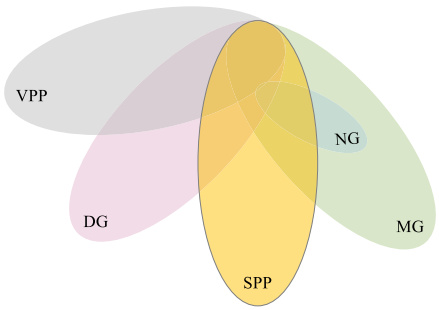

FIGURE 2. Relationships graph.

energy, to supply electric power in aquaculture processes for communities in southern Bangladesh. In [29], an EMS approach is proposed for a MG containing several DG units, residential loads, and production processes. In [14], the authors present an EMS to promote self-consumption in productive processes. The loads of the productive process of all the aforementioned works were represented through a constant-power (CP) load model. However, in general SPPs comprise of voltage-dependent electric loads [14]. Thus, voltage variations in a MG between the normal operating range (i.e., 1 p.u. $\pm 5\%$) [30] may considerably increase or decrease the power consumption of SPPs. For instance, a 5% reduction in voltage can reduce the power consumption of residential loads by approximately 7.6% [31].

Despite the fact that there is extensive research in the field of voltage-dependent load modeling in MGs [30], [32], [33], little attention has been paid to integrating them into SPPs and EMSs. In this context, voltage-dependent models, such as the exponential approach, were proposed in EMS [30], [34]. However, the authors in [13] showed that these models may not be suitable to represent the complex characteristic of SPPs. Additionally, a time-variant ZIP (TV-ZIP) load model was considered in [35]. However, this work assumed certain parameters are already known and did not address the integration of SPPs into an EMS. More recently, in [13] we presented an extended multi-zone ZIP (EMZ-ZIP) load model, which showed a better performance to represent the complex behavior and the voltage sensitivity of the SPPs compared to other approaches. Nevertheless, the full integration of this approach with the EMS was out of the scope of this work. In fact, the change in load modelling can affect the strategy of the EMS in the following ways, e.g., i) reference voltage for DG and storage units for the voltage profile management, and ii) active and reactive power setpoints of dispatchable resources.

Moreover, the understanding of operation logics of this type of complex entities (i.e., SPPs) will lead to better estimations of the consumption required for the optimal operation and planning of future MGs [36]. For instance, an overestimation of consumption could lead to more costly investment decisions and operational expenditures.

To the best of our knowledge the full integration of SPPs into EMSs considering their voltage sensitivity feature and complex behavior is not covered in previous works. One of the reasons that may explain this gap is the introduction of non-convexities in the modeling and the level of information required when the voltage dependency and the realistic representation of the production activities of SPPs are considered.

In this paper, we overcome the aforementioned limitations; thus, we proposed an integration of the SPPs into an AC EMS considering the SPPs' voltage sensitivity. For this purpose, the EMZ-ZIP [13] previously proposed by the authors is considered. This SPP load model has a zoning feature that contributes to manage changes in production activities expected in practical operating scenarios. Moreover, the EMZ-ZIP model involves the introduction of non-convexities in the mathematical formulation of the EMS. Thus, a convex approximation of the EMZ-ZIP is derived to tackle this challenge.

The main contributions of this work are as follows:

i) To the best of our knowledge, this is the first work that integrates SPPs into an EMS approach considering the complex behavior and sensitivity to voltage variations of SPPs.

ii) A novel analysis framework is proposed that integrates SPPs in EMS-MG solutions and provides a better understanding of the consumption of energy required for the optimal operation and planning of future MGs.

iii) Both the previous EMZ-ZIP load model and the parameter identification procedure presented in [13] have been improved. In the former, the model structure was modified by adding a flexible term to better represent the complex behavior of SPPs. In the latter, McCormick's inequalities plus a global optimization (GO) approach are used to identify the parameters of the EMZ-ZIP.

iv) Proposes a zone transition analysis approach to determine the current operating zone candidate for the SPP. This is convenient to address practical operating scenarios such as changes in the scheduling of SPP production activities and expected variability in the solar radiation profile.

To validate the proposed integration methodology, it was applied to test the system that represents a LV isolated MG, which has a low X/R ratio and the integration of an SPP. The results of the technical and economic operation are analyzed to evaluate the performance of the MG when the EMZ-ZIP model is an integral part of the EMS. Furthermore, for comparison purposes, the CP and the TV-ZIP model were used to represent the SPP and were also integrated into the EMS. Note that the abbreviation "ZIP" refers to the representation of a load by its constant-impedance "Z," constant-current "I," and constant-power "P" characteristics [37].

The rest of the paper is organized as follows: Section II presents the proposed framework and methodology. Section III develops the case study, the results, and discussion validating the proposed integration of the SPP into an AC EMS approach. Finally, Section IV highlights the main conclusions of this work.

II. PROPOSED METHODOLOGICAL FRAMEWORK

A. GENERAL DESCRIPTION

To integrate the SPPs into an EMS approach we consider the proposed methodological framework which comprises five main stages depicted in Fig. 3.

In stage 1, a database is established which provides the input information for the following stages. In stage 2, the EMZ-ZIP load model which captures the complex behavior and the voltage dependency feature of the SPPs is developed. Next, once the EMZ-ZIP model has been established, a parameter identification procedure is performed in stage 3. The integration of the SPP model (i.e., the EMZ-ZIP) into an EMS based on a convex transformation and a time zone strategy is addressed in stage 4. Finally, the MG operation based on the proposed EMS integration and a timetable is carried out in stage 5.

Stages 1, 2 and 3 make use of a previous work developed by the authors [13]. Nevertheless, additional improvements and adaptations are incorporated in this work. The description of the stages presented below is focused on these new features. Please refer to our previous work [13] for further details.

In stage 1 we enhanced the content of the ZIP load models database by incorporating information from new devices that may belong to the SPPs. In stage 2, we modified the structure of the EMZ-ZIP model [13] expressed in (1)-(6) by incorporating a flexible generic component (see (3)) to better represent the complex behavior of SPPs. Further, the determination of time zones for the representation of the production process of an SPP is based on the information obtained from the surveys and once identified they remain fixed. However, to have a more accurate time zone determination, we considered an ANN as classification technique [38], [39], and weather variables (e.g., wind speed, ambient temperature, solar irradiation, etc.) as input data for the ANN.

It should be noted that other alternatives exist for the proposed classification. For example, a review including logistic regression, decision trees, support vector machines, among others is presented in [38]. However, according to [39], ANN performs better in terms of accuracy for classification purposes.

For illustrative purposes, let us consider a basic example where an SPP is composed by three devices (cooler, heater, and water pump) represented by ZIP_{cooler}, ZIP_{heater} and ZIP_{pump}, respectively. Then, after applying the ANN to the daily active power profile shown in Fig. 4, three operating zones with their respective active devices are determined. Note that the profile depicted in Fig. 4 is illustrative, however, it is also based on practical experience regarding the actual operation of an SPP installed in Chile [3].

After the time zones have been determined, this information is used in stage 3 for the identification of parameters of the following EMZ-ZIP model,

$$P(k) = ZIP_{flex}(\tilde{V}(k)) + \sum_{\omega \in \Omega_\psi} \delta_\omega(k) ZIP_\omega(\tilde{V}(k)) \tag{1}$$

$$\sum_{\omega \in \Omega_\psi} \delta_\omega(k) \leq 1 \tag{2}$$

$$ZIP_{flex}(\tilde{V}(k)) = P_{flex}(k)(\tilde{\alpha}_1(k)\tilde{V}^2(k) + \tilde{\alpha}_2(k)\tilde{V}(k) + \tilde{\alpha}_3(k)) \tag{3}$$

$$ZIP_\omega(\tilde{V}(k)) = P_{0,\omega}(\alpha_{1,\omega}\tilde{V}^2(k) + \alpha_{2,\omega}\tilde{V}(k) + \alpha_{3,\omega}) \tag{4}$$

$$\tilde{V}(k) = (V(k)/V_0) \tag{5}$$

$$\tilde{\alpha}_1(k) + \tilde{\alpha}_2(k) + \tilde{\alpha}_3(k) = 1 \tag{6}$$

where, $P(k)$ represents the total load (active power) at time step k, $ZIP_{flex}(\tilde{V}(k))$ represents the flexible component of the EMZ-ZIP load model for which it is necessary to identify all its parameters. It should be noted that $ZIP_{flex}(\tilde{V}(k))$ is not part of the aggregate consumption as presented in [13]. This improvement enables a better representation of the complex behavior of SPPs because the $ZIP_{flex}(\tilde{V}(k))$ models the

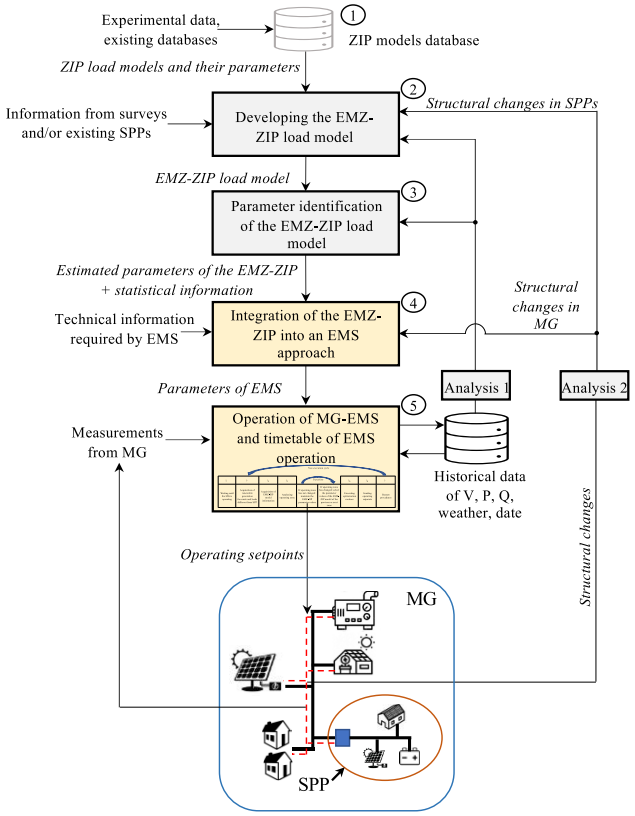

FIGURE 3. Methodological framework for integrating the SPPs into an EMS approach for MGs.

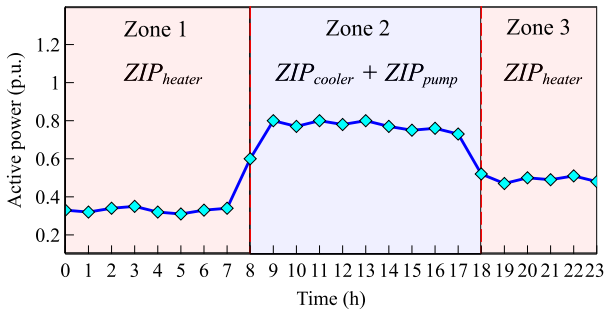

FIGURE 4. Determined operating zones and active devices in each zone.

consumption of SPP devices for which the ZIP parameters are not known. $\delta_\omega(k)$ represents the contribution of the ω-*th* active device to the total power consumption of the SPP. $\delta_\omega(k)$ can assume values between 0 and 1, where the former indicates that a device is not active while the latter indicates that the device is contributing all its power to the total SPP consumption. $P_{flex}(k)$ stands for the nominal active power of the flexible component at nominal voltage, $V(k)$ is the measured voltage at time step k; $\tilde{\alpha}_1(k), \tilde{\alpha}_2(k), \tilde{\alpha}_3(k)$ represent the load features of constant-impedance, constant-current, and constant-power of the flexible component, respectively. Additionally, the term Ω_ψ $\left(\Omega \in \mathbb{Z}^+\right)$ denotes the number of SPPs' active devices in each time zone ψ. It is worth noting that the use of the time zone approach avoids the presence of integer variables in the parameter identification model. Thus, $ZIP_\omega(\tilde{V}(k))$ represents each active device of the SPP in a specific time zone ψ for which its ZIP coefficients (i.e., $P_{0,\omega}$, $\alpha_{1,\omega}$, $\alpha_{2,\omega}$, $\alpha_{3,\omega}$) are already known [13]. Consequently, solely the identification of its contribution (i.e., δ_ω) is needed. It should be noted that, for reactive power representation, an analogous procedure can be used.

In stage 3 we further improved the EMZ-ZIP parameter identification procedure by using a GO approach to increase the probability of reaching the global optimum [40]. In this sense, the Global-Search algorithm [41] and the local solver *fmincon* of MATLAB® [42] are used in this work. Further, the GO approach is highly dependent on the starting point [43]. Thus, it may not be desired that a starting point be close to a non-feasible or local stationary point. Consequently, we used the McCormick's inequalities [44], [45] to determine the starting point for the GO approach.

For a better understanding, the description of stage 4 has been split into the following three subsections: subsection B describes the derivation of the mathematical formulation of the EMS approach, subsection C presents the convexification of the EMZ-ZIP model, and subsection D presents the integration of the model representing the SPPs into the EMS approach. Finally, the description of MG-EMS operation (i.e., stage 5) is presented in section E.

B. EMS GENERAL APPROACH

The economic operation is carried out by the EMS considering the minimization of the overall MG operating costs for a given time horizon K. It is formulated through a mix-integer linear programming (MILP) [46]–[51] as presented in (7)-(19).

$$\underset{P_g(k),P_b(k),P_{US}(k)}{minimize} \sum_{k\in\mathcal{K}} \left(\sum_{g\in\mathcal{G}} C_g P_g(k) + \sum_{b\in\mathcal{B}} C_b P_b(k) + C_{US} P_{US}(k) \right) \Delta_k \tag{7}$$

$$Subject\ to: \sum_{g\in\mathcal{G}} P_g(k) + \sum_{b\in\mathcal{B}} P_b(k) + P_{US}(k) = \sum_{n\in\mathcal{N}} P_{L,n}(k) - \sum_{m\in\mathcal{M}} P_{DG,m}(k) \tag{8}$$

$$v_g^{min} \le v_g(k) \le v_g^{max} \tag{9}$$

$$P_g^{min} \le P_g(k) \le P_g^{max} \tag{10}$$

$$P_b(k) = \eta_b^{dis} P_b^{dis}(k) - \frac{P_b^{ch}(k)}{\eta_b^{ch}} \tag{11}$$

$$0 \le P_b^{ch}(k) \le P_{b,ch}^{max} y_b^{ch}(k) \tag{12}$$

$$0 \le P_b^{dis}(k) \le P_{b,dis}^{max} y_b^{dis}(k) \tag{13}$$

$$y_b^{ch}(k) + y_b^{dis}(k) \le 1 \tag{14}$$

$$y_b^{ch}(k), \quad y_b^{dis}(k) \in \{0, 1\} \tag{15}$$

$$E_b(k) = E_b(k-1) + \Delta_k \frac{P_b^{ch}(k)}{\eta_b^{ch}} - \Delta_k \eta_b^{dis} P_b^{dis}(k) \quad (16)$$

$$E_b^{init} = E_b^{final}(k) \quad (17)$$

$$E_b^{min} \leq E_b(k) \leq E_b^{max} \quad (18)$$

$$P_{US}(k) \geq 0 \quad (19)$$

where Δ_k represents the duration of time sub-period k; C_g and $P_g(k)$ denote the generation cost and the active power provided by the g-th thermal generation unit, respectively; C_b represents the operating cost of the battery. $P_b(k)$ is the power of the battery, assuming a positive value when the battery is injecting power to the MG, and a negative value when the battery is in charging mode. $P_{US}(k)$ and C_{US} stand for the unserved power and the cost of the unserved power in the system, respectively; $P_{L,n}(k)$ is the load consumption in the n-th load center of the system; $P_{DG,m}(k)$ denotes the active power supplied by the m-th DG unit (e.g., PV plant, wind turbine, etc.) Likewise, $v_g(k)$, v_g^{min} and v_g^{max} denote the volume at time step k, minimum and maximum volume of the fuel tank of the g-th thermal generator; P_g^{min} and P_g^{max} are the minimum and maximum limits of active power generated by the i-th thermal generator.

Equation (16) represents a simplified inter-period balance model of the battery [46]. Where $E_b(k)$ represents the total energy stored in the battery. The power $P_b^{ch}(k)$ and $P_b^{dis}(k)$ are used when the battery is charging and discharging, respectively. The parameters η_b^{ch} and η_b^{dis} are used to represent the charge and discharge energy efficiencies of the battery, respectively. $y_b^{ch}(k)$ and $y_b^{dis}(k)$ are the binary variables related to each mode of operation of the b-th battery unit. Equation (14) ensures that only one mode of operation (i.e., charging and discharging) of the b-th battery is active for a specific period. $P_{ch,b}^{max}$ and $P_{dis,b}^{max}$ denote the maximum charging and discharging allowed values of active power of the b-th battery; E_b^{min} and E_b^{max} represent the minimum and maximum allowed values of energy stored by the b-th battery unit, respectively. E_b^{init} and $E_b^{final}(k)$ represent a reference energy value and final energy stored by the b-th battery unit.

It is evident that the EMS formulation in (7)-(19) only considers the active power balance between generation and consumption. However, since the network model is not considered, it is not possible to guarantee that the power scheduled and produced by the generation units will be transferred to the electricity consumption centers [24]. Indeed, the network's constraints are required to achieve a MG operation within the operating voltage limits and power losses restriction [52], [53]. Moreover, because bus voltages are not considered in the EMS formulation above, the voltage sensitivity of the SPPs cannot be fully represented.

Consequently, to address the challenges mentioned above, the network's constraints are added to the EMS formulation. The MG line model consists of the single-line equivalent circuit illustrated in Fig. 5.

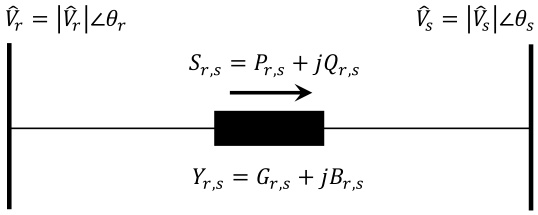

FIGURE 5. MG line model.

If the line power flows from bus r to bus s; then, $S_{r,s}$, $P_{r,s}$ and $Q_{r,s}$ represent the apparent, the active, and the reactive power flowing through the line. Then, the admittance matrix that comprises the complex rectangular representation of all MG line admittances (conductance and susceptance) is denoted as follows:

$$Y_{bus} = G + jB \quad (20)$$

where, G and B represent the conductance and the susceptance, respectively. Additionally, expressing the bus voltages through their polar form as in (21).

$$\hat{V}_r = \left|\hat{V}_r\right| \angle \theta_r \quad (21)$$

Moreover, for the simplicity in notation let $V_r = \left|\hat{V}_r\right|$. Then, the resulting active and reactive powers injected at an arbitrary bus r of the system [54] are expressed as in (22)-(23).

$$P_r(k) = V_r^2(k) G_{r,r} + \sum_{\substack{s \in \mathfrak{B} \\ s \neq r}} \left[V_r(k) V_s(k) G_{r,s} \times \cos(\theta_r(k) - \theta_s(k)) + V_r(k) V_s(k) B_{r,s} \times \sin(\theta_r(k) - \theta_s(k)) \right] \quad (22)$$

$$Q_r(k) = -V_r^2(k) B_{r,r} - \sum_{\substack{s \in \mathfrak{B} \\ s \neq r}} \left[V_r(k) V_s(k) G_{r,s} \times \cos(\theta_r(k) - \theta_s(k)) - V_r(k) V_s(k) B_{r,s} \times \sin(\theta_r(k) - \theta_s(k)) \right] \quad (23)$$

where $\mathfrak{B}$ is the set of buses in the MG, $P_r(k)$ and $Q_r(k)$ represent the difference between generated and demanded power at the r-th bus, $V_r(k)$ is the voltage at the r-th bus, $\theta_r(k)$ represents the voltage angle at the r-th bus. Note that, expressions in (12)-(15) and (22)-(23) are non-convex because they involve integer variables and trigonometric functions (i.e., sine and cosine), respectively. Further, the active and reactive power balance could be achieved through several values of $P_r(k)$, $Q_r(k)$, $V_r(k)$ and $\theta_r(k)$. To efficiently integrate the network equations into the mathematical formulation of the EMS it is required to express them in their convex equivalents. For this reason, we considered the convex approximation proposed in [55].

Power losses are caused because active and reactive currents flow through the lines (i.e., $\zeta_{r,s}$). For notation simplicity, let us define $\ell_{r,s} = \left|\zeta_{r,s}\right|^2$. Then, the current expression is illustrated in (24) and the line active ($P_{r,s}^{loss}(k)$) and reactive

($Q^{loss}_{r,s}(k)$) power losses are expressed in (25) and (26) [56], respectively.

$$\ell_{r,s}(k) = \frac{P^2_{r,s}(k) + Q^2_{r,s}(k)}{V^2_r(k)} \tag{24}$$

$$P^{loss}_{r,s}(k) = \ell_{r,s}(k) \cdot \Re(Y_{r,s}) \tag{25}$$

$$Q^{loss}_{r,s}(k) = \ell_{r,s}(k) \cdot \Im(Y_{r,s}) \tag{26}$$

Further, by following [55], the expressions below are defined:

$$I_{r,s}(k) = V_r(k)V_s(k)\cos(\theta_r(k) - \theta_s(k)) \tag{27}$$

$$T_{r,s}(k) = V_r(k)V_s(k)\sin(\theta_r(k) - \theta_s(k)) \tag{28}$$

$$u_r(k) = \frac{V^2_r(k)}{\sqrt{2}} \tag{29}$$

By substituting $I_{r,s}(k)$, $T_{r,s}(k)$ and $u_r(k)$ and including (24)-(25) in (22)-(23), respectively, we obtain:

$$P_r(k) = \sqrt{2}\,G_{r,r}u_r(k) + \sum_{\substack{s\in\mathfrak{B}\\ s\neq r}}\left[G_{r,s}I_{r,s}(k) + B_{r,s}T_{r,s}(k)\right] + \sum_{\substack{s\in\mathfrak{B}\\ s\neq r}} P^{loss}_{r,s}(k) \tag{30}$$

$$Q_r(k) = -\sqrt{2}\,B_{r,r}u_r(k) - \sum_{\substack{s\in\mathfrak{B}\\ s\neq r}}\left[B_{r,s}I_{r,s}(k) - G_{r,s}T_{r,s}(k)\right] + \sum_{\substack{s\in\mathfrak{B}\\ s\neq r}} Q^{loss}_{r,s}(k) \tag{31}$$

Next, by considering the properties of $\sin(x)$ and $\cos(x)$ the following relations can be derived:

$$I_{r,s}(k) = I_{s,r}(k) \tag{32}$$

$$T_{r,s}(k) = -T_{s,r}(k) \tag{33}$$

$$2u_r(k)\,u_s(k) = I^2_{r,s}(k) + T^2_{r,s}(k) \tag{34}$$

Nevertheless, the expressions in (24) and (34) need to be transformed into their conic programming formats; thus, by following [57] we get:

$$\ell_{r,s}(k)\,u_r(k) \geq P^2_{r,s}(k) + Q^2_{r,s}(k) \tag{35}$$

$$2u_r(k)\,u_s(k) \geq I^2_{r,s}(k) + T^2_{r,s}(k) \tag{36}$$

On the other hand, by adding $P^{loss}_{r,s}(k)$ in (8) yields (37). Besides, since network constraints are considered and these involve reactive power, it is also required to consider the reactive power balance equation (38) in the EMS formulation.

$$\sum_{g\in\mathcal{G}} P_g(k) + \sum_{b\in\mathcal{B}} P_b(k) + P_{US}(k) = \sum_{n\in\mathcal{N}} P_{L,n}(k) + \sum_{\substack{s\in\mathfrak{B}\\ s\neq r}} P^{loss}_{r,s}(k) - \sum_{m\in\mathcal{M}} P_{DG,m}(k) \tag{37}$$

$$\sum_{g\in\mathcal{G}} Q_g(k) + \sum_{b\in\mathcal{B}} Q_b(k) = \sum_{n\in\mathcal{N}} Q_{L,n}(k) + \sum_{\substack{s\in\mathfrak{B}\\ s\neq r}} Q^{loss}_{r,s}(k) \tag{38}$$

Additionally, the constraints of minimum and maximum limits of bus voltages, and maximum power limits through lines are expressed in (39) and (40), respectively.

$$\frac{\left(V^{min}_r\right)^2}{\sqrt{2}} \leq u_r(k) \leq \frac{\left(V^{max}_r\right)^2}{\sqrt{2}} \tag{39}$$

$$\left|Y_{r,s}\left(u_r(k) - u_s(k)\right)\right| \leq S^{max}_{r,s}(k) \tag{40}$$

Consequently, the resulting convex AC multi-nodal EMS optimization problem is formulated as follows:

minimize (7)

Subject to: (37), (38), (30), (31), (9)-(19), (35), (36), (39),

C. CONVEXIFICATION OF THE EMZ-ZIP LOAD MODEL

The EMZ-ZIP expressed in (1)-(6) involves the introduction of non-convexities in the mathematical formulation of the EMS due to the constant-current term of the flexible component, which is non-convex because of the $\tilde{\alpha}_2(k)V_r(k) = \tilde{\alpha}_2(k)\sqrt{u_r(k)}$ relationship after applying the convex approximation to the power flow equations [55]. Therefore, a convex approximation for the EMZ-ZIP model is required. There are two appealing methods in the specialized literature i) the Taylor series approximation method (TAM) [30], and ii) the binomial approximation method (BAM) [58]. It is important to note that these convexification approaches are proved in the cited references and are not part of this work. Therefore, their integration does not require the proof of convergence, but it does require an explanation as to how to apply them to the proposed optimization problem.

Both alternatives can be valid for convexifying the EMZ-ZIP load model. Nevertheless, to determine the most appropriate method, we performed a comparative analysis. This consists of a sensitivity analysis of the relative error of the load representation. More concretely, we took each parameter of the EMZ-ZIP model's flexible component and varied it by taking values from an interval (in this case between 0.01 and 1.00 with a fixed step of 0.01). It should be noted that, to fulfill (6), the difference is equally distributed between the remaining two parameters.

For example, if we consider that the parameter $\tilde{\alpha}_1$(k) will vary, then the resulting expression will be $\tilde{\alpha}_1$ (k) + $\tilde{\alpha}_2$(k)/ 2+$\tilde{\alpha}_3$ (k) /2 = 1. Next, we vary the voltage between 0.85 p.u. and 1.15 p.u. with a fixed step of 0.01 and analyze the relative error between the original EMZ-ZIP model representation and each of the two approximation methods (i.e., TAM and BAM). For the sake of brevity, we only present the plots of the sensitivity analysis for the constant impedance parameter, as given in Fig. 6. In fact, TAM presents a maximum error of around 3%, whereas the BAM presents a maximum error of approximately 0.6%. In the case of the constant-current

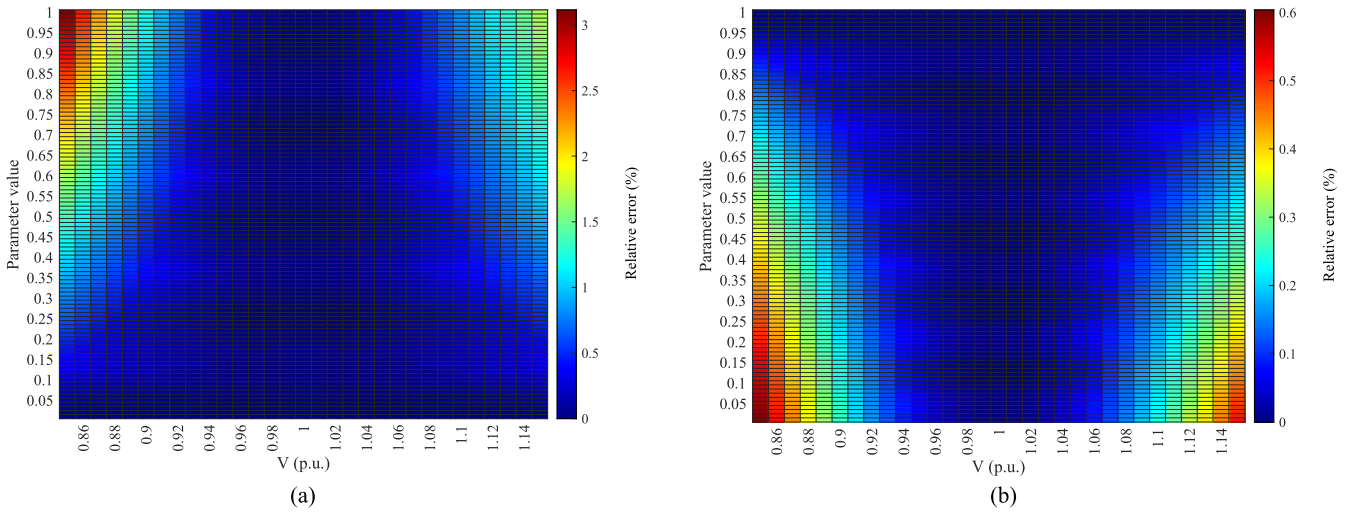

FIGURE 6. Results of the sensitivity analysis for the constant impedance parameter: (a) TAM and (b) BAM.

parameter (not showed in the Fig. 6, but also simulated), the TAM and BAM exhibit a maximum error of 1.29% and 1.32%, respectively. In the case of the constant-power parameter, the BAM has a lower maximum error (0.22%) than the TAM (0.43%). Consequently, the proposed approximation does not affect the precision level of the results.

The BAM outperforms the TAM considering all the cases analyzed in the sensitivity analysis; thus, this method is selected to derive the convex approximation of the EMZ-ZIP load model, and to integrate it into the EMS.

By applying the BAM to the EMZ-ZIP load model, the resulting convex approximation of the EMZ-ZIP model is formulated as follows:

$$P_{SPP}(u_r(k)) \approx ZIP_{flex}(u_r(k)) + \sum_{\omega \in \Omega_\psi} \delta_\omega(k) ZIP_\omega(u_r(k)) \tag{41}$$

$$\sum_{\omega \in \Omega_\psi} \delta_\omega(k) \leq 1 \tag{42}$$

$$ZIP_{flex}(u_r(k)) = P_{flex}(k)\left(\left(\tilde{\alpha}_1(k) + \frac{\tilde{\alpha}_2(k)}{2}\right) u_r(k) + \left(\tilde{\alpha}_3(k) + \frac{\tilde{\alpha}_2(k)}{2}\right)\right) \tag{43}$$

$$ZIP_\omega(u_r(k)) = P_{0,\omega}\left(\left(\alpha_{1,\omega} + \frac{\alpha_{2,\omega}}{2}\right) u_r(k) + \left(\alpha_{3,\omega} + \frac{\alpha_{2,\omega}}{2}\right)\right) \tag{44}$$

It should be noted that the same procedure is applicable to derive the reactive power expression, i.e., $Q_{SPP}(u_r(k))$ of the EMZ-ZIP load model.

D. INTEGRATION OF THE EMZ-ZIP INTO THE EMS APPROACH

Once the EMZ-ZIP has been convexified, its integration into the AC multi-nodal EMS is achieved by replacing $P_{SPP}(u_r(k))$ and $Q_{SPP}(u_r(k))$ in the energy balance expressions (37), (38), and in the load flow expressions (30), (31). Consequently, the resulting active and reactive power balance equations and load flow equations that integrate the convex approximation of the EMZ-ZIP model are shown in Appendix A1.

To avoid the integer variables in (12)-(15), the nonlinear convex BESS model [59] or the convex relaxation proposed in [52] can be considered. The resulting EMS optimization problem is expressed as follows:

minimize (7)

Subject to: (9) − (19), (35), (36), (39), (40), (A1.1)-(A1.4)

Finally, it is important to note that the resulting EMS optimization problem that integrates the EMZ-ZIP load model is convex due to both the BAM applied to the EMZ-ZIP model and the variable transformation used to convexify the power flow constraints and storage. As a result of the above procedure, the EMS became a second-order cone programming (SOCP) optimization problem that can be efficiently solved in a finite number of steps [60] which has a lower computational complexity [61] that scales with the square-root of the problem size [62], i.e., the number of decision variables [63]. Therefore, these properties enable scalability of the resulting EMS and a certain degree of flexibility for its application in actual MGs and large-scale problems [61].

Fig. 8 summarizes the flow of information of the previously described stages that are consistent with the methodological framework depicted in Fig. 3. Firstly, the ANN uses as inputs the weather data and SPP structure information obtained from the surveys to determine the time zones (ψ) for the EMZ-ZIP (stage 2 in Fig. 3). Secondly, the parameters $\left(P_{flex}(k), \tilde{\alpha}_1(k), \tilde{\alpha}_2(k), \tilde{\alpha}_3(k), \delta_\omega(k)\right)$ of the EMZ-ZIP model (1)-(6) are identified for each time zone using the GO strategy (stage 3 in Fig. 3). Lastly, the EMS solves the resulting optimization problem by integrating the convex

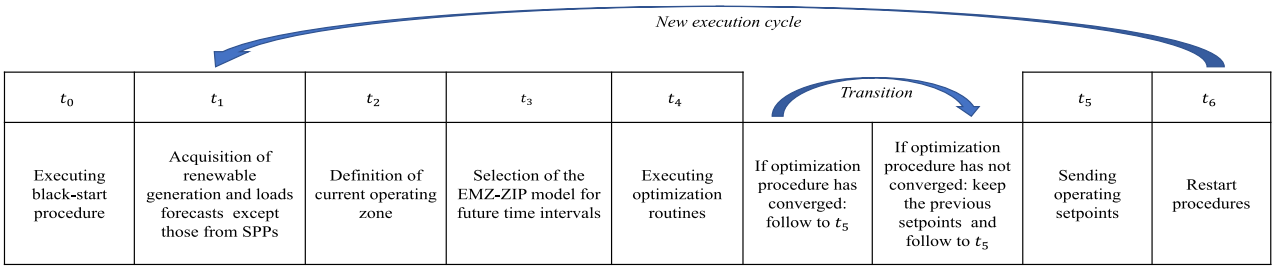

FIGURE 7. Timetable of EMS operation.

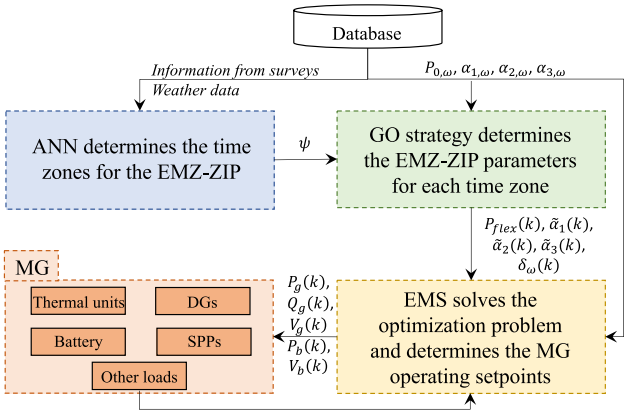

FIGURE 8. Flow chart of the proposed approach.

approximations of the EMZ-ZIP model and determines the operating setpoints $(P_g(k), Q_g(k), V_g(k), P_b(k), V_b(k))$ for the MG dispatchable units (stage 5 in Fig. 3).

E. OPERATION OF MG-EMS

As stated above, the EMS is responsible for determining the optimal (or near optimal) operating setpoints of the dispatchable units present in the MG. With this aim, the timetable in Fig. 7 shows the procedures performed at each EMS run time. At the beginning, i.e., at run time t_0 the EMS is in safe mode. Consequently, a set of predefined settings are stored in the EMS, which is ready to execute a black-start procedure to initiate the operation of the MG [64], [65]. For this purpose, the MG generation units use their local controllers to maintain synchronism in the MG based among others on the droop curves [66]. It should be noted that, at t_0 stages 1, 2, and 3 in Fig. 3 are already developed, which correspond to the EMZ-ZIP model and the identification of its parameters.

Then, at run time t_1 the EMS acquires the renewable generation and load forecasts except for the SPPs. At run time t_2, an EMS routine determines the current operating zone candidate for each SPP based on the predefined zones (see Fig. 4), the local time, and the operating zones determined on stage 2 (see Fig. 3). To achieve this, the EMS routine utilizes the available SPP consumption measurement each time it arrives (e.g., 5, 10 minutes, etc.) and compares it with the two load estimations (e.g., Zone 1 vs Zone 2 EMSZ-ZIPs) in the transition period highlighted in red in Fig. 9. This is done half an hour before and after the transition time. Next, the zone with the lowest error (ε), based on the available measurements, is selected for the SPP load forecast used by the EMS in the transition period. Note that, the duration of the transition period corresponds to a predefined value based on the practical observations of an existing SPP. In t_3, the predefined zone definition is considered for the remaining future time intervals.

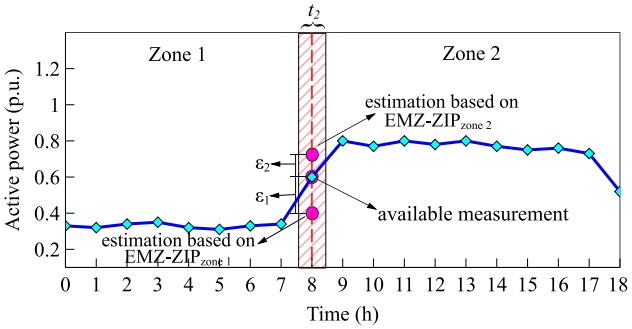

FIGURE 9. Time zone transitions.

Further structural changes in the SPP behavior can be managed by Analysis 1 and 2 blocks presented in Fig. 3. This is a key aspect of the proposal that allows for more robust and efficient management in the transitions between the zones.

Next, at run time t_4 the EMS optimization problem is solved. If the optimization problem converges, the procedure follows to t_5, otherwise the previous operating setpoints are kept. In this run time (i.e., t_5), the valid operating setpoints are sent to the local controllers of dispatchable units in the MG. Specifically, the voltage references and the power generation references are sent using the communication links. It should be noted that in full EMS procedure (t_0-t_5), there is a time difference of approximately 10 minutes. Additionally, in cases of load perturbations (i.e., connection/disconnection), the local controllers react first to maintain the balance between generation and demand. Finally, at run time t_6 the EMS re-start its procedures and goes back to t_1.

III. CASE STUDY

The proposed integration of the SPPs into an EMS approach is tested and validated in a case study. This consists of

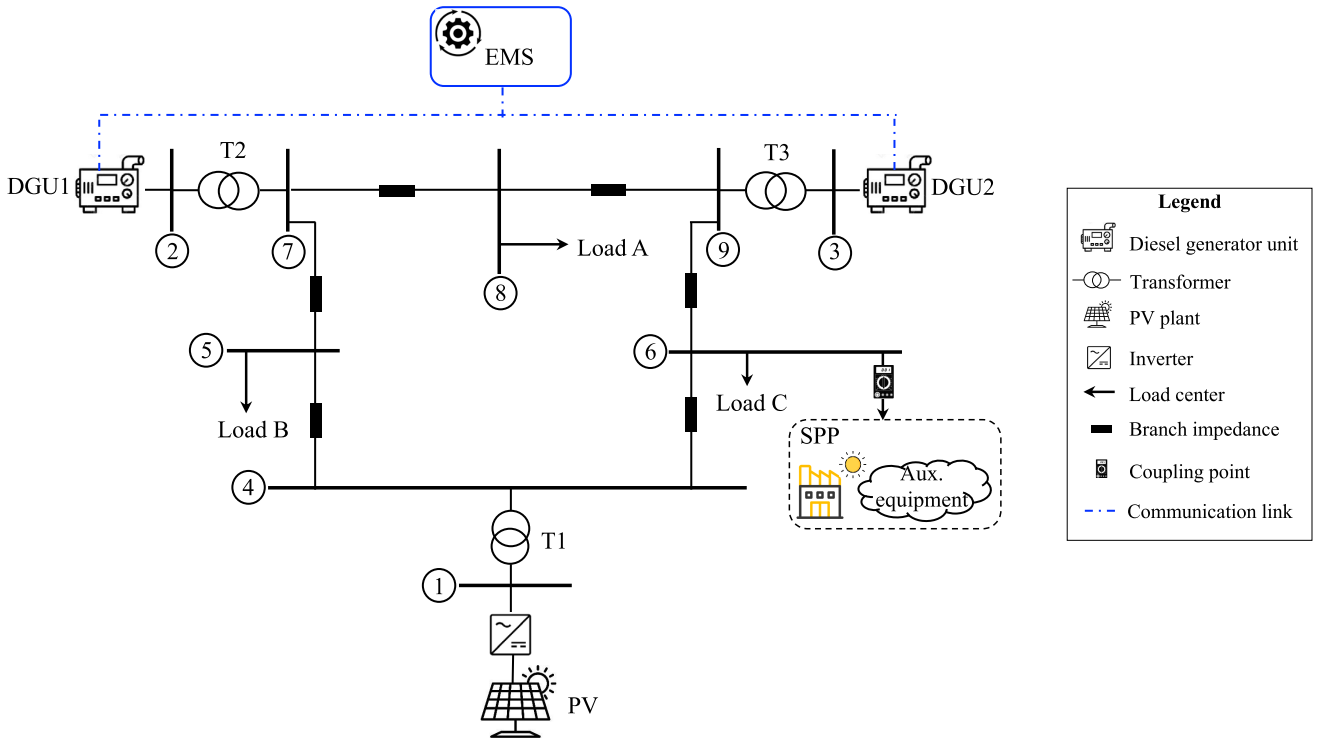

FIGURE 10. Overview of the MG system including an SPP.

a 9-bus test system [67] (see Fig. 10) which was modified to have the characteristics of a low-voltage MG, specially the low X/R ratio [5]. The reference values of the lengths and the X and R values of the MG feeders were taken from [68]. The 9-bus system was selected because its topology is similar to the Huatacondo MG which is an actual isolated system [46], [68] located in northern Chile. As can be seen in Fig. 10, the MG comprises of two diesel-generators units (DGU), three transformers, a PV generator ($\cos \emptyset = 1$) connected to the system through an inverter, and three consumption centers.

Following stages one and two described in Fig. 3, specific information from the SPP process is obtained. In fact, in this case, the SPP was coupled to the MG at bus 6, which consists of a solar drying process (see Fig. 10). It comprises a processing and drying center for fruits and other vegetables and includes an electric heater, a fan, and auxiliary equipment. It should be noted that the SPP is a complex cluster of loads, while the MG is comprised of generation units, loads (including the SPP in Fig. 10 as a complex load) and an EMS to operate autonomously as a single entity.

The considered SPP is a continuous process during the drying period which depends primarily on the air-drying temperature, and humidity [69]. This SPP uses mostly solar radiation to increase the internal temperature of the dryer. On the one hand, during periods of poor solar contribution (e.g., sunrise, sunset, night, cloudy days, etc.), the electric heater is used to maintain the working temperature of the drying process. On the other hand, during periods of high solar contribution, the electric fan is activated primarily to regulate the temperature of the drying process. Further, the auxiliary electric loads are used by offices of the SPP for administrative purposes. These activities are typically carried out from 9:00 a.m. to 6:00 p.m. The SPP electric consumption measurements are collected at the coupling point, as indicated in Fig. 10.

The ZIP parameters for the heater are $\alpha_{1,heater} = 0.92$, $\alpha_{2,heater} = 0.10$, $\alpha_{3,heater} = -0.02$, whereas for the fan they are $\alpha_{1,fan} = 0.26$, $\alpha_{2,fan} = 0.90$, $\alpha_{3,fan} = -0.16$, these parameter values were taken from [70]. In addition, the P_0 parameter values for the electric heater and the electric fan are 2,000 W and 610 W, respectively. The P_0 values of auxiliary equipment can vary between 420 W and 800 W. Those ZIP parameters are stored in the database, which is created at stage 1 (see subsection II-A). Then, following the procedure of stage 2 (see Fig. 3) [13] and considering (1)-(6), the extended ZIP model for the case study is formulated as follows:

$$P(k) = ZIP_{flex}\left(\tilde{V}(k)\right) + \delta_1(k) ZIP_{heater}\left(\tilde{V}(k)\right) + \delta_2(k) ZIP_{fan}(\tilde{V}(k)) \quad (45)$$

$$\sum_{\omega=1}^{2} \delta_\omega(k) \leq 1 \quad (46)$$

$$ZIP_{flex}(\tilde{V}(k)) = P_{flex}(k)\left(\tilde{\alpha}_1(k)\tilde{V}^2(k) + \tilde{\alpha}_2(k)\tilde{V}(k) + \tilde{\alpha}_3(k)\right) \quad (47)$$

Note that $\delta_1(k)$ represents the contribution of the heater and $\delta_2(k)$ represents the contribution of the fan to the power consumption $P(k)$. Besides, because the auxiliary equipment may be turned on/off at any time (influenced by; for example, people's behavior, among others), the flexible component of the EMZ-ZIP model will capture and represent their electrical behavior.

By applying the ANN technique (see subsection II-A), three operating zones were identified. Each zone is comprised of a set of active devices, e.g., in zone 1 the auxiliary equipment and heater are active, in zone 2 the fan and auxiliary equipment may be active, and in zone 3 the heater and auxiliary equipment are active again. After the EMZ-ZIP load model for the case study has been defined, the parameter identification for each zone is performed considering the GO approach. The parameter identification procedure is carried out each 10-minute period of a representative day, i.e., 144 discrete time steps. Further, the input data (i.e., voltage and power measurements) required for the parameter identification procedure are obtained from a simulator of the solar drying SPP, which was built in MATLAB®/Simulink® based on the technical parameters of an actual solar dryer used in this type of production process [71]. Measurements taken every 10 minutes for 8 days are considered, i.e., 1152 samples. From this dataset, measurements of 7 days are used for the parameter identification and the measurements of the remaining day are considered to validate the parameter identification result. The GO approach is implemented using the Global Optimization Toolbox of MATLAB® [72].

The convex AC multi-nodal EMS for the case study is developed considering the EMS mathematical formulation described in subsection II-D. In addition, the EMZ-ZIP expressed in (45)-(47) is integrated into the EMS by using the BAM (see subsection II-D).

The MG depicted in Fig. 10 is modeled in MATLAB®/Simulink® using the Simscape™ Electrical™ Specialized Power Systems blocks [42], which emulates the operation of an actual MG. The electrical part of the DGU is represented by a sixth-order state-space model [73]. The excitation system and the governor of the DGU are based on the IEEE type DC1A excitation system model [74], and the governor block diagram presented in [75], respectively. The transformers are represented by a three-phase two-winding transformer with DY connection [54], [76]. The MG's feeders are similar to those of distribution networks; therefore, they can be represented through a series impedance model [54], [77]. The MG loads, except for the SPP, are modeled as a balanced three-phase load. Besides, the active and reactive power absorbed by the load are proportional to the square of the voltage applied at the load connection bus [78].

The PV plant model is based on a single-stage topology where only one DC/AC converter is used to interface the PV plant to the MG [79]. The DC/AC converter is modeled as a voltage source converter (VSC) which has a decoupled d-q controller [80]. The PV plant power generation is obtained through the mathematical expression provided in [46]. Besides, we assume that the PV plant is always operating following the maximum power point tracker (MPPT). Additionally, the PV system is connected to the MG through a series RL filter. It should be noted that, the model parameter values of all MG elements for the case study are presented in the Appendix A2. Finally, the EMS optimization routine integrating the EMZ-ZIP model is implemented in CVX (a package for specifying and solving convex programs [81], [82]) considering the technical information of the MG elements. Besides, the convex AC multi-nodal EMS optimization problem is solved by using the MOSEK solver [83].

IV. RESULTS AND DISCUSSION

This section presents the results obtained after applying the proposed integration of SPPs in the EMS for the MG of the case study. To simulate the actual operation of the MG, its real-time operation is also evaluated. It is assumed that the DGU1 is responsible for frequency control, whereas the DGU2 can support voltage regulation by acting as a synchronous compensator when it is not producing active power. Two scenarios are considered to evaluate the technical and economic operation of the MG when the SPP is integrated into the EMS: A) operation of MG-EMS, and B) practical performance aspects.

A. OPERATION OF MG-EMS

Operation of the MG is performed continuously during the evaluation window, whereas the EMS minimizes the operational cost of the MG based on available generation and expected load consumption. EMS sends operating setpoints every 10 minutes to local controllers of dispatchable units. A full day of operation (i.e., 24 hours) was considered to analyze the operation of the MG-EMS. To analyze the performance of the EMS for different SPP load models, three cases were developed: i) an EMS including a persistence model with CP [84], ii) an EMS including a TV-ZIP model [85] to represent the SPP, and iii) the previously proposed EMZ-ZIP model (see section II). For comparison purposes, the following performance indicators are considered: i) actual system operating costs and expected EMS operating costs (in Chilean pesos or CLP), ii) reference and operating voltages at the generation buses, iii) and the simulated and estimated power consumption of the SPP. It should be noted that the same PV power generation profile is considered for the three cases, i.e., CP, TV-ZIP and EMZ-ZIP.

Fig. 11 shows the evolution of the actual system operating costs and the expected costs obtained from the EMS for the period of time analyzed (i.e., 24 hours). The relative error between the costs obtained with the CP vs. the other two models is also depicted.

As can be seen in Fig. 11(a), in general, operating costs decrease when the PV plant injects its power generation into the MG approximately between 7:30 a.m. and 7:00 p.m. (19 h). Fig. 11(b) shows a large variation of the relative error after 1:00 p.m. (13 h) between the EMS_{CP} vs $\text{EMS}_{\text{EMZ-ZIP}}$

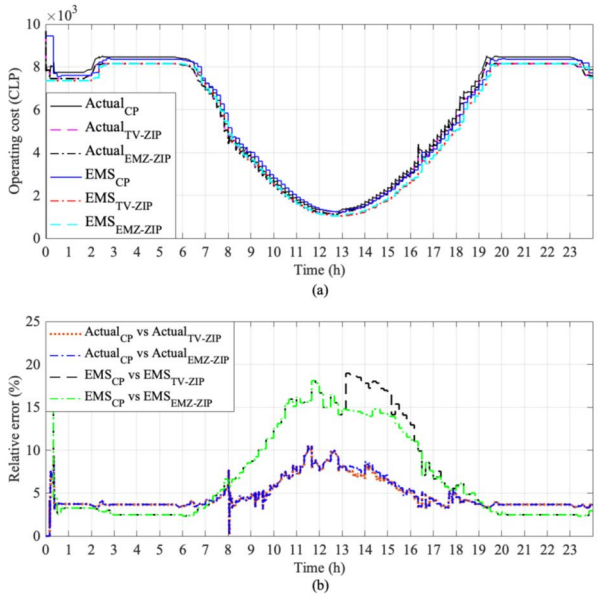

FIGURE 11. (a) Actual system operating and estimated operating costs from the EMS for the three cases (CP, TV-ZIP and EMZ-ZIP), (b) evolution of the relative error between the costs obtained with the CP model vs. TV-ZIP and EMZ-ZIP.

costs, this is because in that zone a device (in this case the fan) was turned on. However, in the parameter estimation stage, the EMZ-ZIP model was able to adequately capture the voltage sensitivity leading to a decrease in the SPP consumption estimation error unlike the TV-ZIP which has a lower estimation performance. For this reason, the relative error EMS_{CP} vs $EMS_{EMZ\text{-}ZIP}$ is smaller than the relative error EMS_{CP} vs $EMS_{TV\text{-}ZIP}$ in such period. Moreover, considerable variations in the $Actual_{CP}$ vs. $Actual_{TV\text{-}ZIP}$ and $Actual_{CP}$ vs. $Actual_{EMZ\text{-}ZIP}$ error at 00:00 and 8:00 a.m. can be seen in Fig. 11(b). The former is because at the beginning of the simulation, the DGUs operate with predefined setpoints that are not provided by the EMS. The latter is because at 8:00 a.m. the work shift starts; therefore, there is a sudden considerable increase in consumption in the SPP.

TABLE 1. Summary of actual MG operating costs.

Load model	Total (CLP)	Min (CLP)	Max (CLP)	Avg. (CLP)	Avg. red (%).
CP	3.927e6	1.232e3	9.677e3	5.843e3	-
TV-ZIP	3.768e6	1.112e3	9.677e3	5.606e3	4.762
EMZ-ZIP	3.767e6	1.112e3	9.677e3	5.605e3	4.800

The summary of the results presented in Table 1 includes the following: total operating cost (Total), minimum cost (Min), maximum cost (Max), average total operating cost for the evaluation day (Avg.), and the average operating cost reduction considering the CP as base case (Avg. red.) Table 2 shows the summary of the operating costs obtained from the EMS for the three cases, considering the same indicators.

TABLE 2. Summary of operating costs obtained from the EMS.

Load model	Total (CLP)	Min (CLP)	Max (CLP)	Avg. (CLP)	Avg. red (%).
CP	3.885e6	1.216e3	9.449e3	5.780e3	-
TV-ZIP	3.689e6	1.044e3	8.149e3	5.489e3	7.447
EMZ-ZIP	3.695e6	1.044e3	8.149e3	5.497e3	7.075

TABLE 3. Summary of the difference between the actual MG operating costs and the costs obtained from the EMS for the three cases of SPP representation.

Load model	Avg. (%)	Min (%)	Max (%)
CP	4.280	0.0024	25.811
TV-ZIP	4.769	0.0053	27.356
EMZ-ZIP	4.361	0.0049	29.356

Table 3 presents a summary of the difference (relative percentage error) between the actual MG operating costs and the costs obtained from the EMS for each case of representation of the SPP power consumption.

The results of actual MG operating costs in Table 1 show that considering load representations that capture the sensitivity of the loads to voltage variations result in a considerable reduction in total MG operating costs by about 5%.

This result is explained by the fact that, when considering voltage sensitive loads, the EMS with an AC approach will try to minimize the voltage at the load buses to reduce the power consumption; thus, reducing the operating costs. This will; consequently, bring the voltages close to the minimum allowed value [30]. It should be noted that the time-variant version of the ZIP model explains its good performance regarding the general cost analysis. The same trend is observed in the operating costs obtained from the EMS (see Table 2). It is worth noting that in this case the TV-ZIP model obtained the highest reduction, which does not match with the actual results from Table 1. This is because the TV-ZIP does not adequately represent the SPP consumption in the EMS. Moreover, the results in Table 3 show that the smallest difference between the actual operating costs and the operating costs estimated from the EMS is obtained with the EMZ-ZIP model (4.361%). This is because the EMZ-ZIP model is better at capturing the SPP's voltage sensitivity; thus, providing a better representation of the SPP's power consumption. In fact, the EMS strategy as depicted in Fig. 13(a) shows that the reference voltage profiles for buses 2 and 3 are adjusted based on the impact of the PV injection during the day, thus achieving a better cost performance. In contrast, in the case of the CP approach, although an AC EMS is considered, the voltage profile is not adjusted properly thus remaining in values near 1 p.u.

Fig. 12(a) shows the results of the reference and generated power of the diesel generators, and the power generation profile of the PV unit. Fig. 12(b) shows the power consumption profile of the SPP simulated in the system, obtained from the

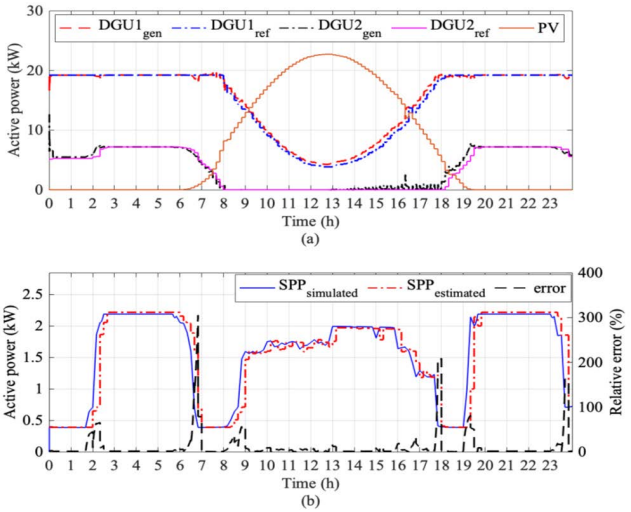

FIGURE 12. (a) Reference and generated power, (b) simulated SPP power consumption profile and estimated SPP consumption obtained from the EMS using the EMZ-ZIP.

EMS using the EMZ-ZIP and the relative error between these two consumption profiles.

As can be seen in Fig. 12(a) the local controllers of the diesel generators are able to follow the power operating setpoints sent from the EMS. In addition, it is observed that the diesel generators decrease their power generation when the PV unit injects its energy production to the system. The SPP consumption profile estimated through the EMZ-ZIP does not show considerable deviations throughout the day (see Fig. 12(b)), except in the following hours 7:00 a.m., 6 p.m. (18h) and 7:00 p.m. (19 h) where considerable changes in SPP consumption occurred. The first change is due to the heater being turned off, the second at the end of the work shift, and the third when the heater is turned on again.

Table 4 summarizes the results of the relative percentage error of the SPP power consumption between simulated and obtained from the EMS using each load model, i.e., CP, TV-ZIP and EMZ-ZIP. The results include the average error (Avg.), minimum (Min), and maximum (Max).

TABLE 4. Summary of the results of the relative percentage error of the SPP power consumption between simulated and obtained from the EMS using each of the load models.

Load model	Avg. (%)	Min (%)	Max (%)
CP	12.515	1.27e-7	294.419
TV-ZIP	12.691	0.0011	305.529
EMZ-ZIP	11.973	0.0013	305.259

The results in Table 4 reveal that, when considering the EMZ-ZIP model to represent the SPP, the average error between the simulated and estimated consumption of the SPP is lower (11.973%) compared to the other load models. This is because the EMZ-ZIP model is better at capturing the SPP's voltage sensitivity which leads to a decrease in error.

Fig. 13(a) displays the results of the reference and operating voltages at the generation buses of the system, and Fig. 13(b) shows the operating voltages at the MG load buses when the SPP load is represented with an EMZ-ZIP.

As can be seen in Fig. 13, in the period when the PV plant injects its power into the system, the voltage at bus 1 increases considerably. This effect is also observed in the other busbars of the system, especially in the nearby busbars 5 and 6. This is because, in this case, the PV plant does not participate in voltage regulation ($\cos \emptyset = 1$); therefore, it requires raising the voltage at bus 1 to deliver its power generation. In addition, the increase in voltage causes an increment in the consumption of the voltage-dependent loads (e.g., SPP). Nevertheless, it is still cheaper to operate the system because of the zero-variable cost of the PV injection and a feasible reduction in the line losses based on an optimized voltage profile provided by the EMS.

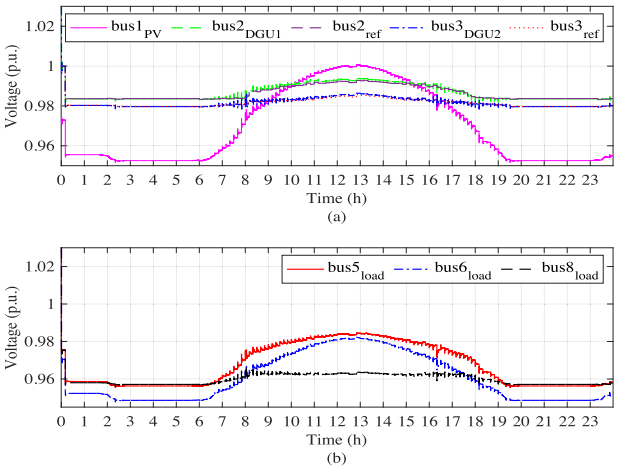

FIGURE 13. (a) Reference and operating voltages at the generation buses of the MG, (b) operating voltages at the load buses of the MG when the SPP power consumption is represented through the EMZ-ZIP load model.

Table 5 presents a summary of the results of the relative percentage error between voltage references and bus voltages at generation buses.

TABLE 5. Summary of the results of the relative percentage error between voltage references and bus voltages at generation buses.

	DGU2			DGU3		
Load model	Avg. (%)	Min (%)	Max (%)	Avg. (%)	Min (%)	Max (%)
CP	0.044	1.23e-5	9.25	0.032	2.02e-5	8.63
TV-ZIP	0.043	1.58e-5	9.25	0.034	4.71e-5	8.63
EMZ-ZIP	0.043	2.37e-5	9.25	0.034	6.18e-5	8.63

Overall, the results depicted in Fig. 13 show that, when considering the operating setpoints sent from the EMS, the voltages at the generation and load buses of the MG are under normal operating ranges. However, the reference voltages sent by the EMS remain close to 1.00 p.u. when the SPP's power consumption is represented through a CP. This is an

expected result because this type of load model does not consider voltage sensitivity. In contrast, as previously mentioned, when voltage-dependent load models (i.e., TV-ZIP or EMZ-ZIP) are considered to represent the SPP, the EMS will try to keep the voltages at the load buses to the minimum allowed value to decrease the load consumption; hence, minimizing the operating costs [30]. Nevertheless, using the EMZ-ZIP model results in a slightly smaller difference between the simulated and reference voltages sent from the EMS (see Table 5).

B. PRACTICAL PERFORMANCE ASPECTS

Clearly, the advantage of considering voltage-dependent load models to represent the SPP is evident given the previously provided results. However, these results showed slight differences between the EMS when integrating either the EMZ-ZIP model or the TV-ZIP model. As a result, to further analyze the performance of the two load modes, we present two additional cases of MG operation that are expected in actual contexts, which are: i) change in the planning of the production activities of the SPP, and ii) variability in the solar radiation profile.

Case 1: In this case, we assume that there is a change in the scheduling of SPP's production activities. More specifically, we consider a change in the morning shift due to the need to produce more products. Therefore, in the new planning, the work shift starts at 8:00 a.m. instead of 9:00 a.m. the usual time. In this context, one day (i.e., 24 hours) of MG operation is simulated including the change in production activities and keeping the MG operating parameters similar to the experiments performed in the previous section.

The experiment consists of representing the SPP consumption in the EMS first through the TV-ZIP model, and then using the EMZ-ZIP that integrates the zone transition approach described in subsection II-E. Moreover, a three-hour analysis window from 7:00 a.m. to 10:00 a.m. is considered, because in this period the effect on the change in the planning of production activities can be better observed. Fig. 14 depicts the reference and generated power of diesel generator units, and the power generation profile of the PV unit, the power consumption profile of the SPP simulated and obtained from the EMS using the TV-ZIP load model for the three-hour period. Fig. 15 shows the same results, but in this case the SPP is represented using the EMZ-ZIP model.

Table 6 summarizes the results of the relative percentage error of the SPP power consumption between what was simulated and obtained from the EMS when using each of the load models considered (i.e., TV-ZIP and EMZ-ZIP) for the whole operating day. Additionally, Table 7 summarizes the results of the relative percentage error of the SPP power consumption between what was simulated and obtained from the EMS when using each load model for the three-hour analysis window. Table 8 gives a summary of the difference between the actual MG operating costs and the costs obtained from the EMS for the three-hour analysis window.

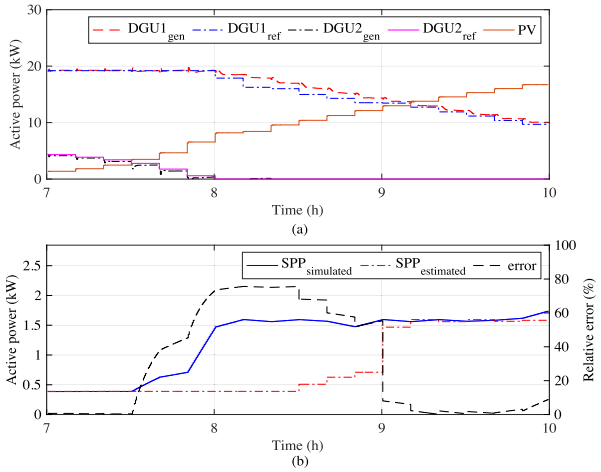

FIGURE 14. (a) Reference and generated power of the diesel generators, and the power generation profile of the PV unit, (b) power consumption profile of the SPP simulated and estimated in the EMS using the TV-ZIP load model for the three-hour period.

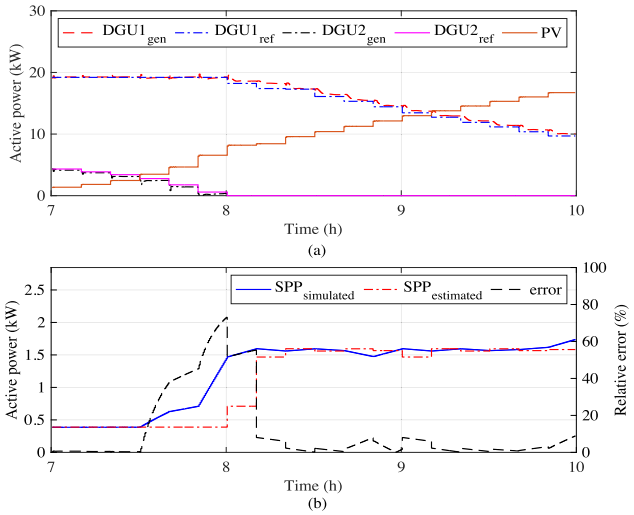

FIGURE 15. (a) Reference and generated power of the diesel generators, and the power generation profile of the PV unit, (b) power consumption profile of the SPP simulated and estimated in the EMS using the EMZ-ZIP load model for the three-hour period.

TABLE 6. Summary of the results of the relative percentage error of the SPP power consumption between what was simulated and obtained from the EMS using each load model.

Load model	Avg. (%)	Min (%)	Max (%)
TV-ZIP	15.215	0.0011	305.529
EMZ-ZIP	12.189	0.0013	305.259

As can be seen in in Fig. 14(b), the ZIP model is not able to identify the change in activity planning; therefore, it presents an accumulated average error by about 45% in the analysis window (see Table 7). In contrast, the EMZ-ZIP model presents a lower average error in the analysis window, specifically 17.198%. This is because the EMS in its routines includes a zone transition analysis (see subsection II-E).

TABLE 7. Summary of the results of the relative percentage error of the SPP power consumption between what was simulated and obtained from the EMS using each load model for the three-hour analysis window.

Load model	Avg. (%)	Min (%)	Max (%)
TV-ZIP	45.205	0.154	75.634
EMZ-ZIP	17.198	0.086	73.038

TABLE 8. Summary of the difference between operating the actual MG operating costs and the costs obtained from the EMS for the three-hour analysis window.

Load model	Avg. (%)	Min (%)	Max (%)
TV-ZIP	3.720	0.141	10.267
EMZ-ZIP	2.511	0.271	8.115

Then, whenever there is a change in the planning of production activities, the EMS can use the zones of the EMZ-ZIP model to advance the beginning of operating zone 2 (see Fig. 15(b)). Thus, this feature presented by the EMZ-ZIP model contributes to decrease the SPP consumption estimation error both in the analysis window (see Table 7), and in the whole operating day (see Table 6) which leads to reducing the error between the actual operating costs of the MG and those expected from the EMS, which in this case is 2.511% (see Table 8).

Case 2: In practical operating scenarios, some variability in the solar resource is expected due to changes in the weather, for example, cloudy days. In this sense, to emulate this scenario, a random variable with uniform distribution is added to the original solar radiation profile. In addition, to evaluate the performance of the two load models (i.e., TV-ZIP and EMZ-ZIP) in representing the SPP consumption under these variable conditions, a sensitivity analysis is performed. This analysis consists of adding the random variable with 10%, 20% or 30% of the value of each solar radiation profile measurement. The sensitivity analysis focuses primarily on the performance of each model in representing SPP consumption, and the difference between the actual operating costs and those obtained from the EMS.

For the sake of brevity, we only present the plots of the MG operation when considering the EMZ-ZIP and for the 30% variability in the solar radiation profile. Fig. 16(a) shows the results of the reference and generated power of the diesel generators, and the power generation profile of the PV unit and Fig. 16(b) shows the power consumption profile of the SPP simulated in the system and obtained from the EMS using the EMZ-ZIP model for 30% variability in the solar radiation profile.

Table 9 presents a summary of the relative percentage error of the SPP power consumption between simulated and obtained from the EMS for the sensitivity analysis, whereas Table 10, summarizes the relative percentage error between the actual MG operating costs and the costs obtained from the EMS. The base case results correspond to those previously obtained with the original solar radiation profile.

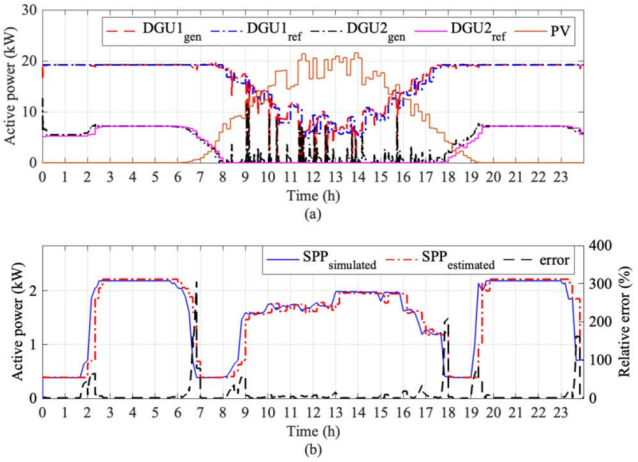

FIGURE 16. (a) Reference and generated power of the diesel generators, and the power generation profile of the PV unit, and (b) power consumption profile of the SPP simulated and obtained from the EMS using the EMZ-ZIP load model for 30% variability in the solar radiation profile.

Overall, the results in Fig. 16(a) show that the variability in the solar radiation profile influences the operating setpoints sent from the EMS, since in certain periods the active power reference of the (i.e., $DGU1_{ref}$) increases/decreases suddenly to cope with such variability. In addition, despite the considerable variability, the local controllers can follow the power references sent from the EMS. However, the DGU2 must generate active power at certain times to maintain the balance between generation and demand, which is affected by the variability of the solar radiation profile.

TABLE 9. Summary of the sensitivity analysis results: relative percentage error of the SPP power consumption between what was simulated and obtained from the EMS.

Solar radiation var.	Load model	Avg. (%)	Min (%)	Max (%)
Base case	TV-ZIP	4.769	0.0053	27.356
	EMZ-ZIP	4.361	0.0049	29.356
10%	TV-ZIP	5.468	0.0015	47.181
	EMZ-ZIP	5.255	0.0019	47.182
20%	TV-ZIP	7.310	0.0030	85.175
	EMZ-ZIP	7.175	0.0024	85.175
30%	TV-ZIP	8.484	0.0039	139.314
	EMZ-ZIP	8.425	0.0039	139.311

Additionally, as expected, the variability in the solar resource considerably influences the performance of the load models when estimating SPP consumption. This is shown in Table 9 since the error between the simulated and estimated power with the TV-ZIP model increases from 4.769% in the base case to 8.484% when the variability is 30%. Similarly, the error between the simulated and estimated power with the EMZ-ZIP model increases from 4.361% to 8.425%. This growth in the SPP power consumption estimation error affects the expected costs in the EMS vs. the actual operating costs of the MG. Nevertheless, in all scenarios of solar profile

TABLE 10. Summary of the sensitivity analysis results: relative percentage error between the actual MG operating costs and the costs obtained from the EMS.

Solar radiation var.	Load model	Avg. (%)	Min (%)	Max (%)
Base case	TV-ZIP	12.691	0.0011	305.529
	EMZ-ZIP	11.973	0.0013	305.259
10%	TV-ZIP	12.722	0.0028	305.309
	EMZ-ZIP	12.001	0.0082	305.309
20%	TV-ZIP	12.733	0.0019	305.356
	EMZ-ZIP	12.022	0.0085	305.356
30%	TV-ZIP	12.746	0.0010	305.300
	EMZ-ZIP	12.039	0.0030	305.300

variability, the EMZ-ZIP load model presents a lower error than the TV-ZIP model (see Table 10).

C. COMPUTATIONAL PERFORMANCE

The computational experiments are conducted on a HP ENVY 27 All-in-One Intel® Core™ i7-4790T @2.70 GHz processor with 12.0 GB RAM, where the MG elements along with the convex AC multi-nodal EMS optimization problem are coded in CVX [81], [82] for MATLAB®, and then subsequently solved using the MOSEK [83] solver. Table 11 shows the computing time required to reach convergence for each case presented above (i.e., operation of MG-EMS, change in planning of production activities and solar radiation variability) and for each model. We ran the computational experiment for each case and for each load model during a 24-hour period. We then average the time taken by the EMS each time it solves the optimization problem, these averages are illustrated in Table 11. Note that the EMS runs every 10 minutes. Thus, it runs 144 times over a 24-hour period. Table 11 shows that, in all the studied cases, the convergence time of the EMS that integrates the EMZ-ZIP model is almost the same as the CP and the TV-ZIP in all cases. This implies that, although the proposed approach is more elaborate, it does not significantly increase the solver time. Therefore, making it feasible for the proposed approach to be implemented on a typical computer used in rural MGs. It should be noted that no convergence problems were observed in all numerical exercises performed with the programmed EMS routines.

TABLE 11. Average time taken by the EMS for each case and for each load model.

Case	Load model	Avg. (sec)
Operation of MG-EMS	CP	1.988
	TV-ZIP	2.039
	EMZ-ZIP	2.043
Change in scheduling of production activities	TV-ZIP	1.865
	EMZ-ZIP	2.025
Solar radiation variability	TV-ZIP	2.202
	EMZ-ZIP	2.001

V. CONCLUSION

In this work, we propose a novel integration of small productive processes into an energy management system approach for microgrids. For this purpose, we extended a previously proposed extended multi-zone ZIP load model. Then, it was integrated into a convex AC multi-nodal energy management system using invertible nonlinear convex transformations and a binomial approximation method, and a time zone procedure. The main conclusions can be summarized as follows:

1) In microgrids, the voltage profile fluctuates due to changes in consumption and distributed generation participation when they inject their power to the system. In addition, small productive processes are complex entities that generally comprise voltage-dependent electrical loads. Thus, not considering the voltage in the load model affects the proper estimation of the small productive process consumption, and the resulting energy management system strategy. In fact, we found that considering the extended multi-zone ZIP model to represent the small productive processes results in a considerable reduction in the total microgrid operating costs (by around 5%), together with an improved voltage profile strategy of the energy management system.
2) The results obtained in our study show the superiority of integrating the extended multi-zone ZIP model to the energy management system when considering operational scenarios expected in practice. For example, changes in the scheduling of the production activities of the small productive process, where the extended multi-zone ZIP presents a lower average error (17.2%) compared to the time-variant ZIP model (45.2%) for the analysis window. In the case of solar variability, the performance of the extended multi-zone ZIP is slightly better (7, 2% error) than the time-variant ZIP model (7, 3%) for 20% of variability in the solar resource.
3) It was shown that the computational effort is similar to energy management system including constant power and ZIP even though the proposed approach is more complex (i.e., energy management system integrating extended multi-zone ZIP). In fact, the maximum average convergence time of the proposed approach (2.043 sec) is almost the same as the energy management system considering the constant power (1.988 sec) and the time-variant ZIP (2.202 sec).

This study, therefore, indicates that the integration of the extended multi-zone ZIP into a convex AC multi-nodal energy management system can properly capture the complex behavior of the small productive processes, and represent the actual operating scenarios of a microgrid that includes a small productive process. This is because microgrid operation exhibits superior technical and economic performance when the extended multi-zone ZIP model is an integral part of

the energy management system. Most notably, this is the first study, to our knowledge, to investigate the integration of small productive processes into an energy management system approach and to consider their complex behavior and their sensitivity to voltage variations.

For further valuable evidence in this field, future work should consider new case studies with additional types of small productive processes as part of the MG-EMS. For instance, small productive processes incorporating distributed generation, storage systems and additional types of loads. Further, the effectiveness of the proposed approach should be verified on case studies with larger microgrids.

Finally, we consider that, in the near future, the integration of the small productive processes into MG-EMSs will increase considerably as a result of the pandemic and the impacts in climate change. This is due to the need for resilient decentralized systems that can be self-sufficient, i.e., systems that can provide water, food, and energy.

APPENDIX

A. APPENDIX A1

Equations (A1.1) and (A1.2) are the resulting active and reactive power balance equations after integrating the convex approximations of the EMZ-ZIP (i.e., $P_{SPP}(u_r(k))$ and $Q_{SPP}(u_r(k))$). Likewise, (A1.3) and (A1.4) denote power flow equations including the convex approximation of the EMZ-ZIP.

B. APPENDIX A2

The PV plant power generation is modeled by the mathematical expression presented in (A2. 1) [46].

$$P_{PV}(k) = \eta_{PV} A_{PV} \Psi(k) \tag{A2.1}$$

where η_{PV} is the solar panel efficiency, A_{PV} denotes the total PV plant surface, and $\Psi(k)$ represents the solar radiation.

TABLE 12. Synchronous machine parameters.

	DGU1	DGU2
Nominal power (kVA)	19.2	12.8
Nominal voltage (Vrms L-L)	220.0	220.0
Xd (p.u.)	1.966	2.057
Xd' (p.u.)	0.200	0.210
Xd'' (p.u.)	0.126	0.132
Tdo' (sec)	4.484	4.489
Tdo'' (sec)	0.068	0.068
Xq (p.u.)	0.977	1.022
Xq'' (p.u.)	0.225	0.236
Tqo'' (sec)	0.100	0.100
Rs (p.u.)	0.061	0.078
Xl (p.u.)	0.079	0.083
H (sec)	1.100	0.900

TABLE 13. Diesel generator excitation system parameters.

	DGU1	DGU2
Ka	400.0	400.0
Kf	0.030	0.030
Ta (sec)	0.020	0.020
Tr (sec)	0.020	0.020
Tf (sec)	1.000	1.000
Vr min (p.u.)	-2.200	-2.200
Vr max (p.u.)	2.200	2.200

TABLE 14. Diesel generator governor parameters.

	DGU1	DGU2
T_1	0.628	3.927
T_2	0.395	15.421
T_3	0.200	0.200
T_4	0.250	0.250
T_5	0.009	0.009
T_6	0.038	0.038
T_d	0.024	0.024
K	0.395	1.69×10^3
K_{droop}	0.100	0.050

$$\sum_{g\in\mathcal{G}} P_g(k) + \sum_{b\in\mathcal{B}} P_b(k) + P_{US}(k) = \sum_{n\in\mathcal{N}} \left[P_{L,n}(k) + P_{SPP}(u_r(k))\right] + \sum_{\substack{s\in\mathfrak{B}\\ s\neq r}} P_{r,s}^{loss}(k) - \sum_{m\in\mathcal{M}} P_{DG,m}(k) \tag{A1.1}$$

$$\sum_{g\in\mathcal{G}} Q_g(k) + \sum_{b\in\mathcal{B}} Q_b(k) = \sum_{n\in\mathcal{N}} \left[Q_{L,n}(k) + Q_{SPP}(u_r(k))\right] + \sum_{\substack{s\in\mathfrak{B}\\ s\neq r}} Q_{r,s}^{loss}(k) \tag{A1.2}$$

$$P_r(k) - P_{SPP}(u_r(k)) = \sqrt{2}\, G_{r,r} u_r(k) + \sum_{\substack{s\in\mathfrak{B}\\ s\neq r}} \left[G_{r,s} I_{r,s}(k) + B_{r,s} T_{r,s}(k)\right] + \sum_{\substack{s\in\mathfrak{B}\\ s\neq r}} P_{r,s}^{loss}(k) \tag{A1.3}$$

$$Q_r(k) - Q_{SPP}(u_r(k)) = -\sqrt{2}\, B_{r,r} u_r(k) - \sum_{\substack{s\in\mathfrak{B}\\ s\neq r}} \left[B_{r,s} I_{r,s}(k) - G_{r,s} T_{r,s}(k)\right] + \sum_{\substack{s\in\mathfrak{B}\\ s\neq r}} Q_{r,s}^{loss}(k) \tag{A1.4}$$

TABLE 15. Transformer parameters.

	T1	T2	T3
Nominal power (kVA)	25.0	25.0	25.0
Nominal primary voltage (Vrms L-L)	220.0	220.0	220.0
Nominal secondary voltage (Vrms L-L)	380.0	380.0	380.0
R1 (p.u.)	0.0015	0.0015	0.0015
L1 (p.u.)	0.0018	0.0018	0.0018
R2 (p.u.)	0.0009	0.0009	0.0009
L2 (p.u.)	0.0025	0.0025	0.0025
Rm (p.u.)	100.0	100.0	100.0
Lm (p.u.)	100.0	100.0	100.0

TABLE 16. Line parameters.

Line		Length (km)	R (Ω/km)	X (Ω/km)
From	To			
4	5	0.20	1.01	0.2525
4	6	0.24	1.01	0.2525
5	7	0.25	1.01	0.2525
6	9	0.38	1.01	0.2525
7	8	0.48	1.01	0.2525
8	9	0.68	1.01	0.2525

TABLE 17. Load parameters.

	Load A	Load B	Load C
Nominal active power (kW)	8.33	9.80	6.86
Nominal reactive power (kVAr)	2.92	3.92	2.40

TABLE 18. Single-stage PV system parameters.

η_{PV} (%)	16.48
A_{PV} (m^2)	121.0
R_f (ohm)	250.0
L_f (henry)	0.6631

REFERENCES

[1] A. Brüderle, B. Attigah, and M. Bodenbender, *Productive Use of Energy PRODUSE: A Manual for Electrification Practitioners*. Eschborn, Germany: European Union Energy Initiative Partnership Dialogue Facility (EUEI PDF), 2011.

[2] *Productive Use of Energy PRODUSE: Measuring Impacts of Electrification on Small and Micro-Enterprises in Sub-Saharan Africa*, GIZ, Eschborn, Germany, 2013.

[3] SERC-Chile. (2021). *Ayllu Solar*. What is Ayllu Solar. Accessed: Dec. 10, 2021. [Online]. Available: https://ayllusolar.cl/en/iniciative/

[4] P. Ramirez-Del-Barrio, P. Mendoza-Araya, F. Valencia, G. Leon, L. Cornejo-Ponce, M. Montedonico, and G. Jimenez-Estevez, "Sustainable development through the use of solar energy for productive processes: The Ayllu solar project," in *Proc. IEEE Global Humanitarian Technol. Conf. (GHTC)*, Oct. 2017, pp. 1–8.

[5] D. E. Olivares, A. Mehrizi-Sani, A. H. Etemadi, C. A. Cañizares, R. Iravani, M. Kazerani, A. H. Hajimiragha, O. Gomis-Bellmunt, M. Saeedifard, R. Palma-Behnke, and G. A. Jiménez-Estévez, "Trends in microgrid control," *IEEE Trans. Smart Grid*, vol. 5, no. 4, pp. 1905–1919, Jul. 2014.

[6] N. Hatziargyriou, H. Asano, R. Iravani, and C. Marnay, "Microgrids," *IEEE Power Energy Mag.*, vol. 5, no. 4, pp. 78–94, Jul./Aug. 2007.

[7] United Nations. *Sustainable Development Goals*. Accessed: Nov. 19, 2021. [Online]. Available: https://sdgs.un.org/es/goals

[8] L. Mayer-Tasch, *Promoting Productive Use of Energy in the Framework of Energy Access Programmes*. Addis Ababa, Ethiopia: Deutsche Gesellschaft für Internationale Zusammenarbeit (GIZ) GmbH, 2013.

[9] S. Booth, X. Li, I. Baring-Gould, D. Kollanyi, A. Bharadwaj, and P. Weston, *Productive Use of Energy in African Micro-Grids: Technical and Bus. Considerations*. Golden, CO, USA: National Renewable Energy Laboratory (NREL), 2018.

[10] J. Terrapon-Pfaff, M.-C. Gröne, C. Dienst, and W. Ortiz, "Productive use of energy—Pathway to development? Reviewing the outcomes and impacts of small-scale energy projects in the global south," *Renew. Sustain. Energy Rev.*, vol. 96, pp. 198–209, Nov. 2018.

[11] P. Ramirez-Del-Barrio, F. Valencia, A. Marconi-Vargas, I. Polanco-Lobos, and P. Mendoza-Araya, "An alpaca fiber processing solution based on solar energy for an isolated location in Chile following a co-construction approach," in *Proc. IEEE Mex. Humanitarian Technol. Conf. (MHTC)*, Mar. 2017, pp. 130–136.

[12] *Solar Energy: Sustainable Development for Arica & Parinacota Semi-annual Y4Q2 Report*, Ayllu-Solar, Santiago, Chile, 2018.

[13] D. Espín-Sarzosa, R. Palma-Behnke, and F. Valencia, "Modeling of small productive processes for the operation of a microgrid," *Energies*, vol. 14, no. 14, p. 4162, Jul. 2021.

[14] J. Barrientos, J. D. López, and F. Valencia, "Adaptive energy management system for self-consumption in productive processes," in *Applied Computer Sciences in Engineering*. Cham, Switzerland: Springer, 2018, pp. 16–27.

[15] N. Hatziargyriou, *Microgrid: Architectures and Control*, 1st ed. Hoboken, NJ, USA: Wiley, 2014.

[16] B. Lasseter, "Microgrids [distributed power generation]," in *Proc. IEEE Power Eng. Soc. Winter Meeting. Conf.*, Jan. 2001, pp. 146–149.

[17] M. S. Pilehvar and B. Mirafzal, "Frequency and voltage supports by battery-fed smart inverters in mixed-inertia microgrids," *Electronics*, vol. 9, no. 11, p. 1755, Oct. 2020.

[18] J.-Y. Kim, J. H. Jeon, S. K. Kim, C. Cho, J. H. Park, H. M. Kim, and K. Y. Nam, "Cooperative control strategy of energy storage system and microsources for stabilizing the microgrid during islanded operation," *IEEE Trans. Power Electron.*, vol. 25, no. 12, pp. 3037–3048, Dec. 2010.

[19] H. M. Ibrahim, M. S. El Moursi, and P.-H. Huang, "Adaptive roles of islanded microgrid components for voltage and frequency transient responses enhancement," *IEEE Trans. Ind. Informat.*, vol. 11, no. 6, pp. 1298–1312, Dec. 2015.

[20] B. Nordman and K. Christensen, "Local power distribution with nanogrids," in *Proc. Int. Green Comput. Conf.*, Jun. 2013, pp. 1–8.

[21] H. Saboori, M. Mohammadi, and R. Taghe, "Virtual power plant (VPP), definition, concept, components and types," in *Proc. Asia–Pacific Power Energy Eng. Conf.*, Mar. 2011, pp. 1–4.

[22] Y. Cao, D. Li, Y. Zhang, Q. Tang, A. Khodaei, H. Zhang, and Z. Han, "Optimal energy management for multi-microgrid under a transactive energy framework with distributionally robust optimization," *IEEE Trans. Smart Grid*, vol. 13, no. 1, pp. 599–612, Jan. 2022.

[23] T. Chen, S. Bu, X. Liu, J. Kang, F. R. Yu, and Z. Han, "Peer-to-peer energy trading and energy conversion in interconnected multi-energy microgrids using multi-agent deep reinforcement learning," *IEEE Trans. Smart Grid*, vol. 13, no. 1, pp. 715–727, Jan. 2022.

[24] G. Liu, T. Ollis, B. Xiao, X. Zhang, and K. Tomsovic, "Community microgrid scheduling considering network operational constraints and building thermal dynamics," *Energies*, vol. 10, no. 10, p. 1554, Oct. 2017.

[25] D. Espín-Sarzosa, R. Palma-Behnke, and O. Núñez-Mata, "Energy management systems for microgrids: Main existing trends in centralized control architectures," *Energies*, vol. 13, no. 3, p. 547, Jan. 2020.

[26] J. Barrientos, J. López, and F. Valencia, "A novel stochastic-programming-based energy management system to promote self-consumption in industrial processes," *Energies*, vol. 11, no. 2, p. 441, Feb. 2018.

[27] Z. Liu, J. Yang, W. Jiang, C. Wei, P. Zhang, and J. Xu, "Research on optimized energy scheduling of rural microgrid," *Appl. Sci.*, vol. 9, no. 21, p. 4641, Oct. 2019.

[28] M. S. U. R. Mahadi, R. Alam, and D. Fernández, "Designing a solar microgrid system for powering an off-grid fish hatchery and nearby households in Bangladesh," in *Proc. AIP Conf.*, 2018, Art. no. 060008.

[29] G. Mohy-ud-din, D. H. Vu, K. M. Muttaqi, and D. Sutanto, "An integrated energy management approach for the economic operation of industrial microgrids under uncertainty of renewable energy," *IEEE Trans. Ind. Appl.*, vol. 56, no. 2, pp. 1062–1073, Mar. 2020.

[30] B. V. Solanki, C. A. Canizares, and K. Bhattacharya, "Practical energy management systems for isolated microgrids," *IEEE Trans. Smart Grid*, vol. 10, no. 5, pp. 4762–4775, Sep. 2019.

[31] M. Farrokhabadi, C. A. Cañizares, and K. Bhattacharya, "Frequency control in isolated/islanded microgrids through voltage regulation," *IEEE Trans. Smart Grid*, vol. 8, no. 3, pp. 1185–1194, May 2017.

[32] B. V. Solanki, K. Bhattacharya, and C. A. Canizares, "Integrated energy management system for isolated microgrids," in *Proc. Power Syst. Comput. Conf. (PSCC)*, Jun. 2016, pp. 1–7.

[33] T. Shekari, S. Golshannavaz, and F. Aminifar, "Techno-economic collaboration of PEV fleets in energy management of microgrids," *IEEE Trans. Power Syst.*, vol. 32, no. 5, pp. 3833–3841, Sep. 2017.

[34] W. Violante, C. A. Canizares, M. A. Trovato, and G. Forte, "An energy management system for isolated microgrids with thermal energy resources," *IEEE Trans. Smart Grid*, vol. 11, no. 4, pp. 2880–2891, Jul. 2020.

[35] D. A. Espín Sarzosa and F. Valencia, "Incorporation of productive solar solutions for communities into microgrid energy management systems," in *Proc. ISES Sol. World Congr.*, 2019, pp. 1–11.

[36] J. Llanos, R. Morales, A. Núñez, D. Sáez, M. Lacalle, L. G. Marín, R. Hernández, and F. Lanas, "Load estimation for microgrid planning based on a self-organizing map methodology," *Appl. Soft Comput.*, vol. 53, pp. 323–335, Apr. 2017.

[37] A. Arif, Z. Wang, J. Wang, B. Mather, H. Bashualdo, and D. Zhao, "Load modeling—A review," *IEEE Trans. Smart Grid*, vol. 9, no. 6, pp. 5986–5999, Nov. 2018.

[38] S. Dreiseitl and L. Ohno-Machado, "Logistic regression and artificial neural network classification models: A methodology review," *J. Biomed. Inform.*, vol. 35, nos. 5–6, pp. 352–359, 2002.

[39] R. Linder, J. Geier, and M. Kölliker, "Artificial neural networks, classification trees and regression: Which method for which customer base?" *J. Database Marketing Customer Strategy Manage.*, vol. 11, no. 4, pp. 344–356, Jul. 2004.

[40] L. Liberti and N. Maculan, *Global Optimization: From Theory to Implementation*, 1st ed. Boston, MA, USA: Springer, 2006.

[41] U. Zsolt, L. Lasdon, J. C. Plummer, F. Glover, J. Kelly, and R. Marti, "Scatter search and local NLP solvers: A multistart framework for global optimization," *INFORMS J. Comp.*, vol. 19, pp. 328–340, Jul. 2007.

[42] *MATLAB and Simulink Release 2020a*, MathWorks-Inc.-Natick, Natick, MA, USA, 2020.

[43] T. Goel and N. Stander, "Adaptive simulated annealing for global optimization in LS-OPT," in *Proc. 7th Eur. LS-DYNA Conf. (LSTC)*, Sacramento, CA, USA, pp. 1–8.

[44] G. P. McCormick, "Computability of global solutions to factorable nonconvex programs: Part I—Convex underestimating problems," *Math. Program.*, vol. 10, no. 1, pp. 147–175, Dec. 1976.

[45] H. Nagarajan, M. Lu, S. Wang, R. Bent, and K. Sundar, "An adaptive, multivariate partitioning algorithm for global optimization of nonconvex programs," *J. Global Optim.*, vol. 74, no. 4, pp. 639–675, Aug. 2019.

[46] R. Palma-Behnke, C. Benavides, F. Lanas, B. Severino, L. Reyes, J. Llanos, and D. Sáez, "A microgrid energy management system based on the rolling horizon strategy," *IEEE Trans. Smart Grid*, vol. 4, no. 2, pp. 996–1006, Jun. 2013.

[47] M. Elsied, A. Oukaour, H. Gualous, R. Hassan, and A. Amin, "An advanced energy management of microgrid system based on genetic algorithm," in *Proc. IEEE 23rd Int. Symp. Ind. Electron. (ISIE)*, Jun. 2014, pp. 2541–2547.

[48] U. B. Tayab, F. Yang, M. El-Hendawi, and J. Lu, "Energy management system for a grid-connected microgrid with photovoltaic and battery energy storage system," in *Proc. Austral. New Zealand Control Conf. (ANZCC)*, Dec. 2018, pp. 141–144.

[49] M. F. Roslan, M. A. Hannan, P. J. Ker, R. A. Begum, T. I. Mahlia, and Z. Y. Dong, "Scheduling controller for microgrids energy management system using optimization algorithm in achieving cost saving and emission reduction," *Appl. Energy*, vol. 292, Jun. 2021, Art. no. 116883.

[50] U. B. Tayab, J. Lu, F. Yang, T. S. AlGarni, and M. Kashif, "Energy management system for microgrids using weighted salp swarm algorithm and hybrid forecasting approach," *Renew. Energy*, vol. 180, pp. 467–481, Dec. 2021.

[51] V. V. S. N. Murty and A. Kumar, "Multi-objective energy management in microgrids with hybrid energy sources and battery energy storage systems," *Protection Control Modern Power Syst.*, vol. 5, no. 1, p. 2, 2020.

[52] M. F. Zia, E. Elbouchikhi, M. Benbouzid, and J. M. Guerrero, "Energy management system for an islanded microgrid with convex relaxation," *IEEE Trans. Ind. Appl.*, vol. 55, no. 6, pp. 7175–7185, Nov. 2019.

[53] M. J. Dolan, E. M. Davidson, G. W. Ault, F. Coffele, I. Kockar, and J. R. McDonald, "Using optimal power flow for management of power flows in active distribution networks within thermal constraints," in *Proc. 44th Int. Universities Power Eng. Conf. (UPEC)*, Sep. 2009, pp. 1–5.

[54] J. J. Grainger, W. D. Stevenson, and G. W. Chang, *Power Systems Analysis*. New York, NY, USA: McGraw-Hill, 2016.

[55] R. A. Jabr, "A conic quadratic format for the load flow equations of meshed networks," *IEEE Trans. Power Syst.*, vol. 22, no. 4, pp. 2285–2286, Nov. 2007.

[56] Z. Q. Wu, "Loss and branch power flow allocation based on topological method," *Electric Power Compon. Syst.*, vol. 30, no. 11, pp. 1179–1193, Nov. 2002.

[57] R. A. Jabr, "Radial distribution load flow using conic programming," *IEEE Trans. Power Syst.*, vol. 21, no. 3, pp. 1458–1459, Aug. 2006.

[58] F. U. Nazir, B. C. Pal, and R. A. Jabr, "Approximate load models for conic OPF solvers," *IEEE Trans. Power Syst.*, vol. 36, no. 1, pp. 549–552, Jan. 2021.

[59] C. Shah and R. Wies, "Algorithms for optimal power flow in isolated distribution networks using different battery energy storage models," in *Proc. IEEE Power Energy Soc. Innov. Smart Grid Technol. Conf. (ISGT)*, Feb. 2020, pp. 1–5.

[60] S. Boyd, S. P. Boyd, L. Vandenberghe, and C. U. Press, *Convex Optimization*. Cambridge, U.K.: Cambridge Univ. Press, 2004.

[61] B. Kocuk, S. Dey, and X. Sun, "Strong SOCP relaxations for the optimal power flow problem," *Oper. Res.*, vol. 64, pp. 1177–1196, May 2016.

[62] M. S. Lobo, L. Vandenberghe, S. Boyd, and H. Lebret, "Applications of second-order cone programming," *Linear Algebra Appl.*, vol. 284, nos. 1–3, pp. 193–228, Nov. 1998.

[63] F. Valencia and A. Marquez, "An economic robust programming approach for the design of energy management systems," in *Power Quality in Future Electrical Power Systems*, 1st ed., S. H. E. A. A. Ahmed and F. Zobaa, Eds. London, U.K.: Institution of Engineering and Technology (IET), 2017, pp. 359–377.

[64] O. Núñez-Mata, R. Palma-Behnke, F. Valencia, A. Urrutia-Molina, P. Mendoza-Araya, and G. Jiménez-Estévez, "Coupling an adaptive protection system with an energy management system for microgrids," *Electr. J.*, vol. 32, no. 10, Dec. 2019, Art. no. 106675.

[65] J. Marchgraber and W. Gawlik, "Investigation of black-starting and islanding capabilities of a battery energy storage system supplying a microgrid consisting of wind turbines, Impedance- and motor-loads," *Energies*, vol. 13, no. 19, p. 5170, Oct. 2020.

[66] W. J. Praiselin and J. B. Edward, "Integrated renewable energy sources with droop control techniques-based microgrid operation," in *Woodhead Publishing Series in Energy*, A. H. Fathima, N. Prabaharan, K. Palanisamy, A. Kalam, S. Mekhilef, and J. J. B. T.-H.-R. E. S. M. Justo, Eds. Sawston, U.K.: Woodhead Publishing, 2018, pp. 39–60.

[67] P. M. Anderson and A. A. Fouad, *Power System Control and Stability*, 2nd ed. Hoboken, NJ, USA: Wiley, 2003.

[68] O. Núñez-Mata, R. Palma-Behnke, F. Valencia, P. Mendoza-Araya, and G. Jiménez-Estévez, "Adaptive protection system for microgrids based on a robust optimization strategy," *Energies*, vol. 11, no. 2, p. 308, Feb. 2018.

[69] C.-G. J. D. Jesús, C. T. Margarita, C.-T. Beatriz, L.-Z. F. Román, M.-P. G. Alberto, and V.-G. C. Jesahel, "Improvements and evaluation on bitter orange leaves (Citrus aurantium L.) solar drying in humid climates," *Sustainability*, vol. 13, no. 16, p. 9393, Aug. 2021.

[70] A. Bokhari, A. Alkan, R. Dogan, M. Diaz-Aguiló, F. de León, D. Czarkowski, Z. Zabar, L. Birenbaum, A. Noel, and R. E. Uosef, "Experimental determination of the ZIP coefficients for modern residential, commercial, and industrial loads," *IEEE Trans. Power Del.*, vol. 29, no. 3, pp. 1372–1381, Jun. 2014.

[71] J. Espinoza S, "Innovación en el deshidratado solar," *Ingeniare. Revista Chilena de Ingeniería*, vol. 24, pp. 72–80, Aug. 2016.

[72] *Global Optimization Toolbox*, MathWorks-Inc.-Natick, Natick, MA, USA, 2020.

[73] The MathWorks-Inc.-Natick. *Synchronous Machine PU Standard*. Accessed: Sep. 27, 2021. [Online]. Available: https://www.mathworks.com/help/physmod/sps/powersys/ref/synchronousmachinepustandard.html

[74] *IEEE Recommended Practice for Excitation System Models for Power System Stability Studies*, Standard 421.5-1992, 1992, pp. 1–56.
[75] S. Sitompul, Y. Hanawa, V. Bupphaves, and G. Fujita, "State of charge control integrated with load frequency control for BESS in islanded microgrid," *Energies*, vol. 13, no. 18, p. 4657, Sep. 2020.
[76] The-MathWorks-Inc.-Natick. *Three-Phase Transformer (Two Windings)*. Accessed: Sep. 27, 2021. [Online]. Available: https://www.mathworks.com/help/physmod/sps/powersys/ref/threephasetransformerthreewindings.html
[77] P. Kundur, *Power System Stability and Control*. New York, NY, USA: McGraw-Hill, 1994.
[78] The-MathWorks-Inc.-Natick. *Three-Phase Parallel RLC Load*. Accessed: Sep. 27, 2021. [Online]. Available: https://www.mathworks.com/help/physmod/sps/powersys/ref/threephaseparallelrlcload.html
[79] L. Lourenço, R. Monaro, M. Salles, J. Cardoso, and L. Quéval, "Evaluation of the reactive power support capability and associated technical costs of photovoltaic Farms' operation," *Energies*, vol. 11, no. 6, p. 1567, Jun. 2018.
[80] M. Worku, M. Hassan, and M. Abido, "Real time energy management and control of renewable energy based microgrid in grid connected and island modes," *Energies*, vol. 12, no. 2, p. 276, Jan. 2019.
[81] M. Grant and S. Boyd. (2013). *CVX: MATLAB Software for Disciplined Convex Programming, Version 2.0 Beta*. [Online]. Available: http://cvxr.com/cvx/
[82] M. Grant and S. Boyd, "Graph implementations for nonsmooth convex programs, recent advances in learning and control (a tribute to M. Vidyasagar)," in *Recent Advances in Learning and Control*, V. Blondel, S. Boyd, and H. Kimura, Eds. Cham, Switzerland: Springer, 2008, pp. 95–110.
[83] *The MOSEK Optimization Toolbox for MATLAB Manual. Version 9.0*, MOSEK ApS, Copenhagen, Denmark, 2019.
[84] C. F. M. Coimbra and H. T. C. Pedro, *Stochastic-Learning Methods*. Amsterdam, The Netherlands: Elsevier, 2013.
[85] M. S. Hossan, H. M. M. Maruf, and B. Chowdhury, "Comparison of the ZIP load model and the exponential load model for CVR factor evaluation," in *Proc. IEEE Power Energy Soc. Gen. Meeting*, Jul. 2017, pp. 1–5.

DANNY ESPIN-SARZOSA (Member, IEEE) was born in Latacunga, Ecuador. He received the Electromechanics Engineering degree from the Universidad de las Fuerzas Armadas-ESPE, Ecuador. He is currently pursuing the Ph.D. degree with the Department of Electrical Engineering, University of Chile. He is also a Researcher at the Energy Center, FCFM, University of Chile. His research interests include load modeling and operation of microgrids, renewable energies, decentralized energy solutions, and the development of solar-based small/medium size rural productive processes.

RODRIGO PALMA-BEHNKE (Senior Member, IEEE) was born in Antofagasta, Chile. He received the B.Sc. and M.Sc. degrees in electrical engineering from the Pontificia Universidad Católica de Chile and the Dr.-Ing. degree from the University of Dortmund, Germany. He is currently a Full Professor with the Department of Electrical Engineering, University of Chile, where he is also the Director of the Energy Center, FCFM, and a PI with the Solar Energy Research Center, Chile. His research interests include the planning and operation of electrical systems in competitive power markets, renewable energy, solar energy solutions, smart grids, power system education, and the development of microgrids solutions.

FELIPE VALENCIA (Member, IEEE) was born in Medellín, Colombia. He received the Control Engineering, master's, and Ph.D. *(magna cum laude)* degrees in control engineering from the Universidad Nacional de Colombia. Currently, he is an Academic Researcher with the Facultad de Ciencias de la Ingeniería, Universidad Austral de Chile. He is also an Associate Researcher with the Solar Energy Research Center, Chile, a member of the Energy Poverty Network (Chile), and a Researcher of the Colombian Energy Transition Initiative Energética 2030. His current research interests include design of distributed and hierarchical strategies for controlling large-scale systems, real-time operation of power systems, and greening small/medium size rural productive processes through renewable energies and circular economy linkage.